A theory of working memory without consciousness or sustained activity

Darinka Trübutschek[1, 2, 3, *], Sébastien Marti [3], Andrés Ojeda[4], Jean-Rémi King[5, 6], Yuanyuan Mi[7], Misha Tsodyks[8, 9], and Stanislas Dehaene[3, 10]

1 – Ecole des Neurosciences de Paris Ile-de-France, 15 rue de l'Ecole de médecine, 75006 Paris, France

2 – Université Pierre et Marie Curie, 4 Place Jussieu, 75005 Paris, France

3 – Cognitive Neuroimaging Unit, CEA DSV/I2BM, INSERM, Université Paris-Sud, Université Paris-Saclay, NeuroSpin center, 91191 Gif/Yvette, France

4 – Department of Zoology, University of Oxford, Oxford OX1 3PS, United Kingdom

5 – Department of Psychology, New York University, 4 Washington Place, New York, USA

6 – Frankfurt Institute for Advanced Studies, Frankfurt, Germany

7 – Brain Science Center, Institute of Basic Medical Sciences, 100850 Beijing, China

8 – Department of Neurobiology, Weizmann Institute of Science, 76100 Rehovot, Israel

9 – Department of Neuroscience, Columbia University, 10032 New York, USA

10 – Collège de France, 11 Place Marcelin Berthelot, 75005 Paris, France

*Correspondence: darinkat87@gmail.com

Abstract

Working memory and conscious perception are thought to share similar brain mechanisms, yet recent reports of non-conscious working memory challenge this view. Combining visual masking with magnetoencephalography, we investigate the reality of non-conscious working memory and dissect its neural mechanisms. In a spatial delayed-response task, participants reported the location of a subjectively unseen target above chance-level after several seconds. Conscious perception and conscious working memory were characterized by similar signatures: a sustained desynchronization in the alpha/beta band over frontal cortex, and a decodable representation of target location in posterior sensors. During non-conscious working memory, such activity vanished. Our findings contradict models that identify working memory with sustained neural firing, but are compatible with recent proposals of 'activity-silent' working memory. We present a theoretical framework and simulations showing how slowly decaying synaptic changes allow cell assemblies to go dormant during the delay, yet be retrieved above chance-level after several seconds.

Introduction

Prominent theories of working memory require information to be consciously maintained (Baars and Franklin, 2003; Baddeley, 2003; Oberauer, 2002). Conversely, influential models of visual awareness hold information maintenance as a key property of conscious perception, highlighting synchronous thalamocortical activity (Tononi and Koch, 2008), cortical recurrence (Lamme and Roelfsema, 2000), or the sustained recruitment of parietal and dorsolateral prefrontal regions (i.e., the same areas as in working memory; Naghavi and Nyberg, 2005) in a global neuronal workspace (Dehaene and Changeux, 2011; Dehaene and Naccache, 2001). Experimentally, non-conscious priming only lasts a few hundred milliseconds (Dupoux et al., 2008; Greenwald et al., 1996) and unseen stimuli typically fail to induce late and sustained cerebral responses (Dehaene et al., 2014). Conscious perception, in contrast, exerts a durable influence on behavior, accompanied by sustained neural activity (King et al., 2014; Salti et al., 2015; Schurger et al., 2015). The hypothesis of an intimate coupling between conscious perception and working memory is thus grounded in theory and supported by numerous empirical findings.

Recent behavioral and neuroimaging evidence, however, has questioned this prevailing view by suggesting that working memory may also operate non-consciously. Unseen stimuli may influence behavior for several seconds (Bergström and Eriksson, 2015; Soto and Silvanto, 2014). Soto and colleagues (2011), for instance, showed that participants recalled the orientation of a subjectively unseen Gabor cue above chance-level after a 5s-delay. Functional magnetic resonance imaging suggests that prefrontal activity may underlie such non-conscious working memory (Bergström and Eriksson, 2014; Dutta et al., 2014).

The verdict for non-conscious working memory is far from definitive, however. Delayed performance with subjectively unseen stimuli was barely above chance (Soto et al., 2011) and could have arisen from a small percentage of errors in visibility reports, with

subjects miscategorizing a seen target as unseen (miscategorization hypothesis). If this were the case, then the blindsight trials, on which subjects correctly identified the target while denying any subjective awareness of the stimulus, should display similar, if not identical, neural signatures and contents as the seen trials. Alternatively, participants could also have ventured a guess about the target as soon as it appeared and consciously maintained this early guess (conscious maintenance hypothesis). Many priming studies have shown that fast guessing results in above-chance objective performance with subjectively unseen stimuli (Merikle, 2001). The observed blindsight effect would then reflect a normal form of conscious working memory (Stein et al., 2016). This alternative hypothesis is hard to eliminate on purely behavioral grounds; it can only be rejected by tracking the dynamics of working memory activity, for instance using brain-imaging, and determining whether this activity occurs immediately after the target even on unseen trials.

Here, we set out to address these issues, focusing on four main objectives: First, we probed the replicability of the long-lasting blindsight effect reported by Soto et al. (2011) as well as its robustness with respect to interference from distraction and a conscious working memory load in order to delineate it from other forms of prolonged iconic or sensory memory. Second, we interrogated the link between conscious perception and conscious working memory, examining whether the maintenance period in working memory could be likened to a prolongation of a conscious episode. Third, we tested the reality of non-conscious working memory by systematically examining the neural correlates of the blindsight effect and using them to assess the two above alternative hypotheses (the miscategorization and conscious maintenance hypothesis). Lastly, we propose a neuronal theory to offer a mechanistic account of conscious and non-conscious working memory.

Results

We combined magnetoencephalography (MEG) with a spatial masking paradigm to assess working memory performance under varying levels of subjective visibility (Figure 1A and Methods). On 80% of the trials, a target square was flashed in 1 of 20 locations and then masked. Subjects were asked to localize the target after a variable delay (2.5 – 4.0s) and to rate its visibility on a scale from *1* (not seen) to *4* (clearly seen). On the remaining 20% of trials, the target was omitted, allowing us to contrast brain activity between target-present and -absent trials. A visible distractor square was presented 1.5s into the delay period on half the trials, challenging participants' resistance to distraction and enabling us to evaluate the robustness of the blindsight effect behaviorally. In addition to this working memory task, subjects also completed a perception-only control condition without the delay and target-localization periods (perception task), so that we could isolate brain activity specific to conscious perception (without a working memory requirement) and investigate its link with working memory.

Behavioral maintenance and shielding against distraction

We first examined objective performance in the working memory task as a function of target visibility. Overall, subjects reported the exact target location with high accuracy on seen trials (collapsed across visibility ratings > *1*: $M_{correct}$ = 69.1%, $SD_{correct}$ = 17.4%; chance = 5%; $t(16) = 15.2$, $p < .001$, 95% CI = [55.2%, 73.1%]; Cohen's $d = 3.7$). As subjective visibility of the target increased from glimpsed (visibility = *2*) to clearly seen (visibility = *4*), there was a corresponding monotonic increase in accuracy (Figure 1B; ps < .05 for all pair-wise comparisons). Crucially, performance remained above chance even on unseen trials (rating = *1*: $M_{correct}$ = 22.4%, $SD_{correct}$ = 13.8%; $t(16) = 5.2$, $p < .001$, 95% CI = [10.3%, 24.4%]; Cohen's $d = 1.3$). This blindsight remained substantial after a 4s-delay ($M_{correct}$ = 21.1%, $SD_{correct}$ = 14.7%; $t(16) = 4.5$, $p < .001$, 95% CI = [8.5%, 23.7%]; Cohen's $d = 1.0$).

Spatial distributions of participants' responses were concentrated around the target (Figure 2A). To correct for small errors in localization, we computed the rate of correct responding with a tolerance of two positions (+/- 36°) surrounding the target location. In subjects displaying above-chance blindsight (chance = 25%; $p < .05$ in a χ^2-test; $n = 13$), we estimated the precision of working memory as the standard deviation of the distribution within this tolerance interval (Methods). Performance was better on seen than on unseen trials, both in terms of rate of correct responding ($F(1, 16) = 198.5$, $p < .001$; partial $\eta^2 = .925$) and precision ($F(1, 12) = 36.7$, $p < .001$; partial $\eta^2 = .754$). There was neither an effect of the distractor on these measures (all ps > .079), nor any significant interactions between distractor and visibility (all ps > .251), indicating that distractor presence did not affect retention for seen or unseen targets. Restricting the analyses to trials within one position of the actual target location (+/- 18°) or to the subgroup of 13 subjects included in the MEG analyses did not change these findings qualitatively.

While target detection *d*' exceeded chance-level ($M = 1.5$, $SD = 0.7$; $t(16) = 8.9$, $p < .001$, 95% CI = [1.2, 1.9]; Cohen's $d = 2.1$) and correlated with accuracy and the rate of correct responding on seen trials (both Pearson rs > .762, both ps < .001), there was no relationship between our participants' sensitivity to the target and any of our performance measures on the unseen trials (all Pearson rs < .342, all ps > .179; Figure 2 – Figure Supplement 1A). Thus, target visibility predicted performance in the objective working memory task only on seen trials, but not on unseen trials.

Overall, these results confirm, with much higher non-conscious performance, the observations of previous studies (Soto et al., 2011): Non-conscious information may be maintained for up to 4 seconds and successfully shielded against distraction from a salient visual stimulus, independently of overall subjective visibility.

Resistance to conscious working memory load and delay duration

To probe the similarity between conscious working memory and the observed long-lasting blindsight effect, in a second behavioral experiment with 21 subjects, we examined whether imposing a load on conscious working memory (remembering digits) affected non-conscious performance. On each trial, 1 (low load) or 5 (high load) digits were simultaneously shown for 1.5s, followed by a 1s-fixation period and the same sequence of events (target and mask) as in experiment 1. After a variable delay (0 or 4s), participants had to (1) localize the target, (2) recall the digits in the correct order, and (3) rate target visibility.

Subjects again chose the exact target position with high accuracy on seen trials ($M_{correct}$ = 77.8%, $SD_{correct}$ = 13.9%) and remained above chance on unseen trials ($M_{correct}$ = 25.6%, $SD_{correct}$ = 11.8%; chance = 5%; $t(18) = 7.6$, $p < .001$, 95% CI = [14.9%, 26.3%]; Cohen's $d = 1.7$). While, as in experiment 1, cue detection d' was greater than chance (M = 1.7, SD = 0.8; $t(20) = 10.2$, $p < .001$, 95% CI = [1.4, 2.1]; Cohen's $d = 2.2$), no correlations were observed with objective task performance on the unseen trials (all Pearson rs < .366, all ps > .115; seen trials: all Pearson rs > .443, all ps < .051; Figure 2 – Figure Supplement 1B). As expected, participants were better at recalling 1 rather than 5 digits in the correct order (M = 93.3% vs. 89.5%, $F(1, 17) = 4.7$, $p = .045$), irrespective of target visibility or delay duration (all ps > .135).

Analyzing only the trials with correctly recalled digits, we observed an impact of load on the precision with which target location was retained ($F(1, 13) = 7.3$, $p = .018$; partial η^2 = .360). Crucially, load modulated the relationship between precision and visibility (interaction $F(1, 13) = 8.7$, $p = .011$; partial η^2 = .400), with no effect on seen ($t(13) = 0.6$, $p = .561$) and a strong reduction of precision on unseen trials ($t(13) = -3.6$, $p = .004$). There was no effect of working memory load on the rate of correct responding (all ps > .229; Figure 2B).

Delay duration (0 or 4s) also did not influence the rate of correct responding (all ps > .082; Figure 2C). It did, however, affect overall precision ($F(1, 15) = 9.3$, $p = .008$; partial η^2

= .383) and the relationship between precision and visibility (interaction $F(1, 15) = 5.2$, $p = .037$; partial $\eta^2 = .259$). This interaction was driven by higher precision on no-delay than on 4s-delay trials, exclusively when subjects had seen the target ($t(15) = -5.7$, $p < .001$; unseen trials: $t(15) = -0.6$, $p = .559$).

Overall, these results highlight the replicability and robustness of the long-lasting blindsight effect and suggest that it does not just constitute a prolonged version of iconic memory: Even in the presence of a concurrent conscious working memory load, unseen stimuli could be maintained, with no detectable decay as a function of delay. However, the systems involved in the short-term maintenance of conscious and non-conscious stimuli interacted, because a conscious verbal working memory load diminished the precision with which non-conscious spatial information was maintained.

Similarity of conscious perception and conscious working memory

To tackle our second objective – a detailed examination of the link between conscious perception and conscious working memory –, we turned to our MEG data and first ensured that the mechanisms underlying conscious perception were stable across experimental conditions. The subtraction of the event-related fields (ERFs) evoked by unseen trials from those evoked by seen trials revealed similar topographies for the perception and working memory task (Figure 3A): Starting at ~300ms and extending until ~500ms after target onset, a response emerged over right parieto-temporal magnetometers. This divergence resulted primarily from a sudden increase in activity on seen trials ("ignition") in the perception ($p_{FDR} < .05$ from 384 – 416ms and from 504 – 516ms) and working memory task ($p_{FDR} < .05$ from 328 – 364ms and from 396 – 404ms; Figure 3B). The observed topographies and time courses fall within the time window of typical neural markers of conscious perception, including the P3b (e.g., Del Cul et al., 2007; Salti et al., 2015; Sergent et al., 2005). Consciously perceiving the target stimulus therefore involved comparable neural mechanisms, irrespective of task.

We next directly probed the relationship between conscious perception and information maintenance in conscious working memory. Does the latter reflect a prolonged conscious episode, or does it involve a distinct set of processes recruited only during the retention phase? If conscious working memory can indeed be likened to conscious perception, one might expect the same patterns that index such perception to be sustained throughout the working memory maintenance period. Linear multivariate pattern classifiers were trained to predict visibility (seen or unseen) from MEG signals separately for each task. Classification performance was assessed during an early time period (100 – 300ms), the critical P3b time window (300 – 600ms), and the first (0.6 – 1.55s) and second part (1.55 – 2.5s) of the delay period.

Decoding of the visibility effect was comparable in the two tasks (Figure 3C and Table 1): Classification performance rose sharply between 100 and 300ms and peaked during the P3b time window (all *p*s < .007, except 100 – 300ms in the working memory task, where $p = .066$). It then decayed slowly from ~1s onwards in both tasks, yet remained above chance during the 0.6 – 1.55s interval (all *p*s < .001). Similar time courses were also observed when training in one task and testing for generalization to the other. Though rapidly dropping to chance-level after ~1s, classifiers trained in the perception task performed above chance during the first three time windows on working memory trials (and vice versa; all *p*s < .014), indicating that, early on, both tasks recruited similar brain mechanisms.

Temporal generalization analyses (King and Dehaene, 2014) were used to evaluate the onset and duration of patterns of brain activity. If working memory were just a prolonged conscious episode, classifiers trained at time points relevant to conscious perception (e.g., the P3b window) should generalize extensively, potentially spanning the entire delay. Our findings supported this hypothesis only in part. The temporal generalization matrix for the working memory task presented as a thick diagonal, suggesting that brain activity was mainly

characterized by changing, but long-lasting patterns. Though failing to achieve statistical significance over the entire 0.6 – 1.55s interval (all *p*s > .101), at a more lenient, uncorrected threshold, classifiers trained during the P3b time window (300 – 600ms) in the working memory task remained weakly efficient until ~692ms (AUC = 0.54 +/- 0.02, $p_{\text{uncorrected}}$ = .023). Similarly, classifiers trained during the same time period in the perception task and tested in the working memory task persisted up to ~860ms (AUC = 0.53 +/- 0.01, $p_{\text{uncorrected}}$ = .028). Brain processes deployed for the conscious representation of the target were thus partially sustained during the working memory delay. The reverse analysis, in which we trained classifiers during the retention period in the working memory task (0.8 – 2.5s), did not reveal any generalization to the P3b time window in the perception task (p = .101).

These results confirm that seeing the target entailed a similar unfolding of neural events in two task contexts: Conscious perception primarily consisted in a dynamic series of partially overlapping information-processing stages, each characterized by temporary, metastable patterns of neural activity. The same neural codes appeared to be recruited at the beginning of the maintenance period (up to ~1s). As such, these findings corroborate previous accounts linking conscious perception to an "ignition" of brain activity (Del Cul et al., 2007; Gaillard et al., 2009; Salti et al., 2015; Sergent et al., 2005) and suggest that, in part, working memory implies the prolongation of a conscious episode, and, in part, a succession of additional processing steps.

A sustained decrease in alpha/beta power distinguishes conscious working memory

Our focus so far has been on evoked brain activity. However, other reliable neural signatures of conscious perception have been identified in the frequency domain (Gaillard et al., 2009; Gross et al., 2007; King et al., 2016; Wyart and Tallon-Baudry, 2009). We thus turned to time-frequency analyses and first contrasted seen trials with both our target-absent control condition as well as unseen trials in both tasks (Figure 4A and Figure 4 – Figure

Supplement 1A). In order to qualify as a signature of conscious perception, any candidate characteristic should exist in the perception-only control condition (without any working memory requirement) and be specific to seen trials. Cluster-based permutation analyses singled out a desynchronization in the alpha band (8 – 12Hz) as the principal correlate of conscious perception in the perception task (seen – target-absent: p_{clust} = .004; seen – unseen: p_{clust} = .009), with seen trials displaying a strong decrease in power (relative to baseline) compared to either the target-absent or the unseen trials. Initially left-lateralized in centro-temporal sensors, this effect moved to fronto-central channels and extended between ~300 and 1700ms. A similar, albeit later (500 – 1700ms) and more bilateral fronto-central, desynchronization was also observed in the beta band (13 – 30Hz; seen – target-absent: p_{clust} < .001; seen – unseen: p_{clust} = .01). No differences between the unseen and target-absent trials were found in the alpha (p_{clust} > .676) or beta band (p_{clust} > .226, apart from a short-lived, weak difference between ~0.9 and 1.3s, where p_{clust} = .020), suggesting that unseen trials strongly resembled trials without a target.

Most importantly, when comparing seen and target-absent/unseen trials in the working memory task, we again observed a similar, but now temporally sustained, pattern of alpha/beta band desynchronization (Figure 4B and Figure 4 – Figure Supplement 1B). Starting at ~300 to 500ms, seen targets evoked a power decrease in central, temporal/parietal, and frontal regions in the alpha (seen – target-absent: p_{clust} = .003; seen – unseen: p_{clust} = .003) and beta band (seen – target-absent: p_{clust} = .009; seen – unseen: p_{clust} < .001). Crucially, this desynchronization spanned the entire delay period and was specific to seen trials (Figure 4A), with no differences in power between the unseen and target-absent trials in either band (alpha: p_{clust} > .729; beta: p_{clust} > .657) and only a couple of interspersed periods of residual desynchronization persisting in the target-absent control trials. No task- or visibility-related modulations in power spectra were found in occipital areas, and the desynchronization

originated primarily from a parietal network of brain sources (Figures 4A and B). In conjunction with the afore-mentioned results, these findings imply that alpha/beta desynchronization is a correlate of conscious perception (Gaillard et al., 2009) and a neural state common to conscious perception and conscious working memory.

A distinct neurophysiological mechanism for non-conscious working memory

Having identified markers of conscious perception and working memory in both multivariate and time-frequency analyses, we can now test the reality of non-conscious working memory by confronting it with several alternative hypotheses. The miscategorization hypothesis suggests that the long-lasting blindsight resulted from a small set of seen trials erroneously labeled as unseen. Unseen correct trials should thus display similar neural signatures as seen trials, including a shared discriminative decoding axis and a desynchronization in the alpha/beta band. An analogous reasoning holds for the conscious maintenance hypothesis, according to which the observed blindsight effect arises from the conscious maintenance of an early guess: Conscious processing would occur on unseen trials and we should thus find a sustained decrease in alpha/beta power similar to the one on seen trials. Conversely, a clear distinction between brain responses on seen trials and on unseen (correct) trials would suggest that blindsight resulted from a distinct non-conscious mechanism of information maintenance.

We first probed the alternative hypotheses with the ERF data. Training a decoder to distinguish seen from unseen trials in the perception task and applying it to the unseen correct and incorrect trials in the working memory task, we directly assessed the classifier's ability to generalize from seen to unseen correct trials (accuracy decoder). If, indeed, the latter had actually been seen, such a decoder should look similar to the above-described generalization analysis, in which a classifier had been trained on seen/unseen trials in the perception task and tested on the same labels in the working memory task (visibility decoder). As shown in Figure

4 – Figure Supplement 2A, this was not the case. Whereas the temporal generalization matrix for the visibility decoder presented as a thick diagonal, no discernable pattern emerged for the accuracy decoder. The time courses of diagonal decoding were also quite dissimilar. For the visibility decoder (see also above), classification performance first rose above chance at ~148ms (AUC = 0.54 +/- 0.01, p_{FDR} = .023), peaked at ~640ms (AUC = 0.58 +/- 0.02, p_{FDR} = .001), and then decayed rapidly by ~1s (first three time windows, all *p*s < .001). In contrast, classification for the accuracy decoder was erratic and transient: It first sharply peaked at ~180ms (AUC = 0.55 +/- 0.01, $p_{uncorrected}$ = .037), dropped to chance-level, and then exceeded chance between ~372 and 724ms with a peak at 444ms (AUC = 0.57 +/- 0.02, $p_{uncorrected}$ = .007). Much unlike any of the previous decoders involving the perception task, long after the visibility response, it rose a third time between ~1.44 and 1.74s, peaking with similar magnitude as before at ~1.58s (AUC = 0.57 +/- 0.02, $p_{uncorrected}$ = .010; P3b and last time window: all *p*s < .023). Although the level of noise evident in the accuracy decoder thus precludes any definitive conclusion, the visibility and accuracy decoders had little in common, rendering it unlikely for the unseen correct trials to have simply been mislabeled.

We next turned to time-frequency analysis. When averaging over all unseen trials in the working memory task, there was no indication of a desynchronization remotely comparable to the one on seen trials (Figure 4A and Figure 4 – Figure Supplement 1C). Indeed, Bayesian statistics indicated that, on the unseen trials, evidence for the null hypothesis (i.e., no relative change in alpha/beta power) was at least similar (at the very end of the epoch) or stronger than evidence for the alternative hypothesis. By contrast, on seen trials, evidence for the alternative hypothesis was always strongly favored (Figure 4 – Figure Supplement 3). Even when analyzing the unseen correct trials separately, there was no appreciable trace of any alpha/beta desynchronization (Figure 4C and Figure 4 – Figure Supplement 3). Only one short-lived effect, reversed relative to conscious trials, was observed in the alpha band (p_{clust} =

.040) in a set of posterior central sensors, corresponding to primarily occipital sources: Starting at ~1.5s and extending until ~1.9s, unseen correct trials exhibited a stronger *increase* in alpha power than their incorrect counterparts. Given the difference in performance on these two types of unseen trials, such small variations are not surprising and could, perhaps, reflect a stronger suppression of interference from the distractor on the unseen correct trials. Unseen correct trials thus appeared to be nearly indistinguishable from the unseen incorrect and target-absent trials.

As multivariate analyses might be more sensitive than univariate ones in detecting similarities between conditions, we also performed the above decoding analysis separately for average alpha (8 – 12 Hz) and beta (13 – 30 Hz) power. Overall, these analyses confirmed our previous findings, albeit more clearly so in the alpha than in the beta band. A visibility decoder trained on alpha power to distinguish seen from unseen trials in the perception task and tested in the working memory task again exhibited a thick diagonal, with above-chance diagonal decoding between ~180ms and 1.18s (first three time windows: all ps < .016). There was no evidence for any generalization to the unseen correct trials (Figure 4 – Figure Supplement 2B; all time windows: ps > .211). Similarly, a visibility decoder trained on average beta power entirely failed to generalize to the unseen correct trials (Figure 4 – Figure Supplement 2C; all time windows: ps > .191). Considering the weak, although statistically significant (all four time windows, ps <= .05), initial generalization from the perception to the working memory task, probably due to the slightly later onset of the beta desychronization in the former, this failure is less informative than the one observed in the alpha band and should be replicated in future investigations.

Taken together, we found a clear distinction in the brain responses of seen and unseen (correct) trials. Converging evidence from our decoding analyses in the ERFs and alpha/beta band suggests that there was no apparent discriminative axis shared between the seen and the

unseen correct trials. Similarly, the desynchronization in alpha/beta power characterizing the seen targets did not emerge on the unseen (correct) trials. These findings therefore argue against the miscategorization and conscious maintenance hypotheses and instead suggest that non-conscious working memory is a genuine phenomenon, distinct from conscious working memory.

Contents of conscious and non-conscious working memory can be tracked transiently

We next set out to identify the neural mechanisms supporting both conscious and non-conscious working memory and first determined where and how the specific contents of working memory were stored. Circular-linear correlations between the amplitude of the ERFs and target location (across all working memory trials) revealed a strong and focal association (relative to a permuted null distribution) over posterior channels, starting at ~120ms and lasting until 904ms (early and P3b time windows: all *ps* < .001; all BFs > 109.60; Figure 5A and Tables 2 and 3). Similarly, distractor position could be tracked between ~194 and 570ms after its presentation (early and P3b time windows: all *p*s < .009; all BFs > 14.47). The position of our stimuli could thus be faithfully retrieved in visual areas.

In a subsequent step, we investigated how target location would be maintained in the context of conscious and non-conscious working memory (Figure 5B). Target position was transiently encoded via slowly decaying activity in occipital as well as bilateral temporo-occipital cortex from ~120 to 800ms on seen trials (early and P3b time windows: all *p*s < .001 and all BFs > 24.07, with the exception of the 100 – 300ms period in right temporo-occipital channels, where $p = .064$ and BF = 2.31) and in occipital and left temporo-occipital brain areas from ~180 to 504ms on unseen trials (early time window: all *p*s < .047; all BFs > 2.58). A clear correlation with target location was therefore found for both seen and unseen trials. In fact, although it was more short-lived on the latter, it was of comparable magnitude as the one observed on the seen trials during the early time window (occipital/left temporo-occipital

channels: all *p*s > .110 when directly comparing the correlation scores of seen and unseen trials in a Wilcoxon signed-rank test). In the case of seen trials, both occipital and left temporo-occipital cortex also maintained the target representation at least throughout the first part of the delay period (all *p*s < .024; all BFs > 3.77), though, intriguingly, this was not accompanied by continuously sustained activity. Target "decodability" instead waxed and waned, appearing and disappearing periodically. No such activity was observed for the maintenance of unseen targets (first and second part of the delay: all *p*s > .446; all BFs < .047). This absence of "decodability" during the maintenance period persisted, even when considering unseen correct and unseen incorrect trials separately (Figure 5C). There was only a trace of residual decoding of target location on unseen correct trials in left temporo-occipital areas during the delay period, but this did not reach significance, potentially due to the low number of trials in this condition. Note that in the perception task, seen targets could be retrieved similarly to their counterparts in the working memory task between ~232 and 1184ms in occipital and bilateral temporo-occipital regions (all *p*s > .068, except for the 100 – 300ms time window in occipital channels where $p = .008$, when directly comparing the correlation scores of seen targets in both tasks in a Wilcoxon signed-rank test; Figure 5 – Figure Supplement 1).

Given the univariate nature of the circular-linear correlations, one might again wonder whether a multivariate strategy would be more sensitive in detecting subtle associations between the MEG data and target location. We therefore used linear support vector regressions (SVR) to predict target angle from the MEG signal as a function of visibility (Methods). As can be seen in Figure 5 – Figure Supplement 2, this method resulted in similar, albeit more noisy, time courses as the ones obtained with the circular-linear correlations: Seen targets were again encoded and maintained intermittently between ~268ms and 1.4s (P3b time window and first part of the delay: *p*s < .05). No statistically significant decoding emerged for

unseen target location. Due to the fact that subjects responded correctly on approximately half of all unseen trials (see Table 4 for average trial counts), we attempted to evaluate the dynamics of the encoding and maintenance of unseen correct and incorrect target locations by training the regression model on the strongest case, the seen correct trials, and applying it separately to the unseen correct and incorrect trials. We again observed no evidence for any generalization at all (Figure 5 – Figure Supplement 3A), though this likely reflects the sensitivity of the analysis more so than any meaningful effect.

Taken together, in line with previous research (Harrison and Tong, 2009; King et al., 2016), these results suggest that posterior sensory regions may initially encode seen and unseen memoranda via slowly decaying neural activity. In the case of conscious working memory, these then seem to be maintained by those same areas through an intermittently reactivated, neural code (Fuentemilla et al., 2010). In contrast, no such periodically resurfacing activity appears to accompany non-conscious working memory.

Further evidence against the conscious maintenance hypothesis

The correlation between target location and brain activity affords an additional way to interrogate the conscious maintenance hypothesis. If subjects quickly guessed the location of an unseen target and then held it in conscious working memory, in addition to observing a signature of conscious processing on the unseen trials, we should observe a correlation with the location of their response long before it occurs. Potentially, remembering the response might recruit brain systems completely different from the ones representing the target.

Circular-linear correlations rendered this prediction unlikely. Associations between response location and the MEG signal were again primarily confined to posterior channels, with more frontal areas being recruited preferentially at the time of the response (Figure 6A). As such, the topographical patterns were highly similar to the ones observed for the correlation with target location. Importantly, no additional regions were identified on the

414 unseen trials and none of these areas showed any appreciable correlation before the
415 presentation of the response screen (Figure 6 – Figure Supplement 1). This suggests that,
416 irrespective of stimulus visibility, common brain networks supported memories for the target
417 stimulus and the ensuing decision and that, in the case of non-conscious working memory,
418 these did not come online until the response.
419 The time courses of the circular-linear correlations further solidified this interpretation
420 (Figure 6B). On seen trials, response position was maintained throughout the majority of the
421 epoch in occipital and left temporo-occipital brain areas (first three time windows: all *p*s <
422 .020; all BFs > 4.16). This was not the case on the unseen trials: No correlation patterns
423 appeared in any of the posterior channels during the course of the epoch (all time windows:
424 all *p*s > .064; all BFs < 1.32). In contrast, a strong correlation emerged for both seen and
425 unseen trials during the response period (0 – 800ms with respect to the onset of the letter cue).
426 Response location could be tracked with similar time courses and magnitude on seen and
427 unseen trials in occipital, bilateral temporo-occipital, and frontal channels (all *p*s < .024; all
428 BFs > 13.73; when directly comparing the correlation scores of seen and unseen targets in a
429 Wilcoxon signed-rank test: all *p*s > .216, except for left temporo-occipital channels, where *p* =
430 .040). When we further distinguished unseen correct from unseen incorrect trials, the results
431 remained similar, though much noisier (Figure 6C): There was no clear correlation pattern
432 before the onset of the response screen on either the unseen correct or the unseen incorrect
433 trials (all *p*s > .096; all BFs < 1.47). Only after the appearance of the letter cues did we
434 observe a correlation with response location.
435 Multivariate decoding analyses confirmed this picture: Whereas response location for
436 seen targets could be tracked similarly to actual target location at least throughout the first
437 part of the delay period (P3b time window and first part of the delay: *p*s < .05; Figure 6 –
438 Figure Supplement 2), no such pattern was observed on the unseen trials (all *p*s > .153). This

absence of decodability persisted on the unseen correct and incorrect trials, even when training the regression model on the seen correct trials (Figure 5 – Figure Supplement 3B).

Overall, these results are incompatible with the hypothesis that the long-lasting blindsight is only due to the conscious maintenance of an early guess, as, in this case, brain responses linked to the subjects' response should have been observed shortly after the presentation of the target stimulus.

Short-term synaptic change as a neurophysiological mechanism for conscious and non-conscious working memory

What mechanism might permit above-chance recall without any continuously sustained brain activity? Recent modelling suggests that sustained neural firing may not be required to maintain a representation in conscious working memory. Mongillo, Barak, and Tsodyks (2008) proposed a theoretical framework for working memory, in which information is stored in calcium-mediated short-term changes in synaptic weights, thus linking the active cells coding for the memorized item. Once these changes have occurred, the cell assembly may go dormant during the delay, while the synaptic weights are slowly decaying. At the end of the delay period, a non-specific read-out signal may then suffice to reactivate the assembly. Furthermore, reactivation of the assembly may also occur spontaneously during the retention phase, similar to the rehearsal process postulated by Baddeley (2003), thus refreshing the weights and permitting the bridging of longer delays. Could this 'activity-silent' mechanism also constitute a plausible neural mechanism for non-conscious working memory?

To test this hypothesis, we simulated our experiments using a one-dimensional recurrent continuous attractor neural network (CANN) based on Mongillo et al. (2008). The CANN encoded the angular position of the target and was composed of neurons aligned according to their preferred stimulus value (Figure 7A). Transient short-term plasticity between the recurrent connections, with a 4s-decay constant, was implemented as described

by Mongillo and colleagues (2008; Figure 7B). Timing of the simulated events was comparable to the experimental paradigm: A target signal was briefly presented at a random location, followed by a mask signal to all neurons and a non-specific recall signal after a 3s-delay.

If the activity-silent mechanism constituted a plausible neurophysiological correlate of conscious and non-conscious working memory, these simulations should capture our principal findings. A stimulus presented at threshold should entail one of two different maintenance regimes: a first distinguished by near-perfect recall with spontaneous reactivations of the memorized representation throughout the retention period (thus resembling the prolonged, yet fluctuating, "decodability" of seen target locations), and a second characterized by above-chance objective performance in the almost complete absence of delay activity (thereby portraying the time course of the circular-linear correlations for the unseen stimuli).

In a noiseless model, there indeed existed a critical value of mask amplitude, A_{critical}, which separated two distinct regimes: Just as was the case for our seen trials, when $A_{\text{mask}} < A_{\text{critical}}$, the neural assembly coding for the target spontaneously reactivated during the delay (Figure 7C). However, when $A_{\text{mask}} > A_{\text{critical}}$, the system evolved into a state without spontaneous activation of target-specific neurons, yet with a reactivation in response to a non-specific recall signal, mimicking our unseen trials (Figure 7D). When fixing mask amplitude near A_{critical} and adding noise continuously or just to the inputs, the network exhibited both types of regimes in nearly equal proportions: 50.8% of trials were characterized by an activity-silent delay interspersed with spontaneous reactivations and 49.2% by an entirely activity-silent delay period. Reminiscent of our behavioral results, sorting the trials according to the existence or absence of these reactivations and computing the histograms of recalled target position relative to true location produced two distributions of objective working memory performance: one, in which target position was nearly accurately stored (Figure 7E),

and one, in which performance remained above chance despite a higher base rate of errors (Figure 7F). These simulations replicate our experimental findings (in particular Figures 2 and 5) and suggest the activity-silent framework as a likely candidate mechanism for both conscious and non-conscious working memory.

Discussion

Conscious perception and working memory are thought to be intimately related, yet recent evidence challenged this assumption by proposing the existence of non-conscious working memory (Soto et al., 2011). The present results may reconcile these views. Both conscious perception and conscious working memory shared similar signatures, including an alpha/beta power decrease, the latter spanning the entire delay on working-memory trials. However, participants remained able to localize a subjectively invisible target after a 4s-delay. We found no evidence that this long-lasting blindsight could simply be explained by erroneous visibility reports or by the conscious maintenance of an early guess. It thus likely reflects genuine non-conscious working memory. Despite the inherent differences in subjective experience for conscious and non-conscious working memory, a single, activity-silent mechanism might support both conscious and non-conscious information maintenance. We now discuss these points in turn.

Shared brain signatures underlie conscious perception and conscious working memory

Consistent with introspective reports and research on visual awareness and working memory (Baddeley, 2003; Dehaene et al., 2014), we observed a close relationship between conscious perception and maintenance in conscious working memory. In both tasks, classifiers trained to separate seen and unseen trials resulted in thick diagonals up to ~1s after target onset, even when generalizing from one task to the other. Such long diagonals have repeatedly been observed in recent studies and are thought to reflect sequential processing (King and Dehaene, 2014; Marti et al., 2015; Salti et al., 2015; Stokes et al., 2015; Wolff et

al., 2015). Irrespective of context, conscious perception and early parts of conscious maintenance thus involve a similar series of partially overlapping processing stages.

Time-frequency decompositions reinforced and extended this conclusion. Seen trials in the perception task were distinguished from both a target-absent control condition and unseen trials by a prominent decrease in alpha/beta power over fronto-central sensors, corresponding to a distributed network centered on parietal cortex. A similar desynchronization, sustained throughout the retention period, was also observed for conscious working memory. Alpha/beta band desynchronizations such as these have previously been linked with conscious perception (Gaillard et al., 2009; Wyart and Tallon-Baudry, 2009) and working memory (Lundqvist et al., 2016). Modelling suggests that the memorized item is encoded by intermittent gamma bursts, which interrupt an ongoing desynchronized beta default state (Lundqvist et al., 2011). Such a decreased rate of beta bursts, once averaged over many trials, would have resulted in the apparently sustained power decrease we observed. Increases in gamma power have also been shown in some studies on conscious perception (e.g., Gaillard et al., 2009), but we failed to detect it here, perhaps because our targets were brief, peripheral, and low in intensity.

Circular-linear correlations further highlighted the similarity between conscious perception and working memory. Location information could be tracked for ~1s on perception-only trials and for at least 1.5 seconds of the working memory retention period. The mental representation formed during conscious perception was therefore either maintained or repeatedly replayed during conscious working memory.

Long-lasting blindsight effect reflects genuine non-conscious working memory

Even when subjects indicated not having seen the target, they still identified its position much better than chance up to 4 seconds after its presentation. This long-lasting blindsight effect was replicated in two independent experiments and exhibited typical

properties of working memory, withstanding salient visible distractors and a concurrent demand on conscious working memory. Those results corroborate previous research showing that information can be maintained non-consciously (e.g., Bergström and Eriksson, 2014; Bergström and Eriksson, 2015; Dutta et al., 2014; Soto et al., 2011). However, these prior findings could have arisen due to errors in visibility reports. If, for example, a participant had been left with a weak impression of the target (and, consequently, its location), he or she might not have had adequate internal evidence to refer to this perceptual state as seen, thus incorrectly applying the label unseen. A small number of such errors would have produced above-chance responding. Another explanation could have been the conscious maintenance of an early guess, whereby subjects would have ventured a prediction as to the correct target position immediately after its presentation and then consciously maintained this hunch.

The MEG results provide evidence against these possibilities. First, whereas seen trials were characterized by a sustained desynchronization in the alpha/beta band in parietal brain areas, no comparable desynchronization was observed on unseen trials, even when subjects correctly identified the target location. On the contrary, the only, short-lived, difference between unseen correct and unseen incorrect trials emerged around the time of the distractor and was reversed in direction: Unseen correct trials were accompanied by an increase in power in the alpha band with respect to their incorrect counterpart, an effect that might relate to a successful attempt to reduce interference from the distractor (Cooper et al., 2003; Jensen and Mazaheri, 2010). Otherwise, unseen correct and incorrect trials were indistinguishable in their power spectra and similar to the target-absent control condition. Second, there was no clear evidence for a shared discriminative decoding axis between the seen and the unseen correct trials: Generalization was entirely unsuccessful when the classifier was trained on the time-frequency data, and highly dissimilar from the original visibility decoder when trained on the ERFs. While it is impossible to draw definitive conclusions just from the current

dataset and future research should replicate these results, the majority of our evidence thus points against an interpretation, in which the unseen correct trials constituted either just a subset of seen trials, or arose from the conscious maintenance of an early guess. Instead, inasmuch as the observed desynchronization serves as a faithful indicator of conscious processing, it argues in favor of a differential state of non-conscious working memory with a distinct neural signature.

Circular-linear correlations as well as multivariate regression models between the amplitude of the MEG signal and response location support this interpretation. On seen trials, response position was coded akin to target location: Initially maintained via slowly decaying neural activity in posterior brain areas, the response code subsequently resurfaced intermittently in the same as well as more frontal regions. There was no detectable evidence for such a code on the unseen trials. Only during the very last part of the delay, right before the response, did response-related neural activity emerge and ramp up to the same level as on seen trials during the response period. As such, the absence of any prior delay-period activity does not appear to be an artifact attributable to low statistical power or an increase in noise on the unseen trials. Instead, in conjunction with the absence of any signature of conscious processing on these trials, these findings imply that subjects did not consciously maintain an early guess and rather relied on genuine non-conscious working memory to perform the task.

In this context, an interesting avenue for future investigations might be to delineate the boundary conditions of such non-conscious working memory. Although the short-term maintenance of information certainly lies at the heart of most theories of working memory (Eriksson et al., 2015), there exist additional criteria for working memory that were not investigated in the present study. It is thus an interesting empirical question whether these other working memory processes may also occur without subjective awareness. Is it, for example, possible to manipulate information non-consciously? Though speculative, in light of

589 the proposed activity-silent code for non-conscious maintenance (without any spontaneous
590 reactivations; see below), it seems unlikely. Being an entirely passive process, it is not clear
591 how stored representations could be transformed without being persistently activated and thus
592 becoming conscious. Future research is, however, needed to provide a definitive answer.

593 **A theoretical framework for 'activity-silent' working memory**

594 Target-related activity was not continuously sustained throughout the delay period,
595 even when the target square had been consciously perceived. It instead fluctuated,
596 disappearing and reappearing intermittently. This feature was even more pronounced on the
597 unseen trials, with no evidence for any such retention-related activity beyond ~1s. We
598 presented a theoretical framework, based on Mongillo et al. (2008) and the concept of
599 'activity-silent' working memory (Stokes, 2015), that may provide a plausible explanation for
600 maintenance without sustained neural activity. According to this model, short-term memories
601 are retained by slowly decaying patterns of synaptic weights. A retrieval cue presented at the
602 end of the delay may then serve as a non-specific read-out signal capable of reactivating these
603 dormant representations above chance-level. Support for this model comes from experiments
604 in which non-specific, task-irrelevant stimuli (Wolff et al., 2017, 2015), neutral post-cues
605 (Sprague et al., 2016), or transcranial magnetic stimulation (TMS) pulses (Rose et al., 2016)
606 presented during a delay restore the decodability of representations. Direct physiological
607 evidence for the postulated short-term changes in synaptic efficacies also exists (Fujisawa et
608 al., 2008).

609 The present non-conscious condition provides further support for such an activity-
610 silent mechanism. In this framework, a stimulus that fails to cross the threshold for sustained
611 activity and subjective visibility may still induce enough activity in high-level cortical circuits
612 to trigger short-term synaptic changes. Such transient non-conscious propagation of activity
613 has indeed been simulated in neural networks (Dehaene and Naccache, 2001) and measured

experimentally in temporo-occipital, parietal, and even prefrontal cortices (Salti et al., 2015; van Gaal and Lamme, 2012). In the present work, we indeed observed some residual, transiently decodable activity over left occipito-temporal sensors on unseen correct trials. The memory of target location could therefore have arisen from posterior visual maps (Roelfsema, 2015), although future research should test this prediction further. Note that activity-silent mechanisms need not apply solely to prefrontal cortex as originally proposed by Mongillo et al. (2008), but constitute a generic mechanism that may be replicated in different areas, possibly with increasingly longer time constants across the cortical hierarchy (Chaudhuri et al., 2014). Only some of these areas/spatial maps may be storing the information on unseen trials.

A key feature of Mongillo et al.'s (2008) model and the present simulations is that, even for above-threshold ('seen') stimuli, delay activity is not continuously sustained. Occasional bouts of spontaneous reactivation instead refresh the synaptic weights and maintain the memory for an indefinite time. The time courses of the circular-linear correlations and of the multivariate decoding we observed on seen trials match this description: While target location was encoded and maintained in temporo-occipital areas, target "decodability" was not constantly sustained, but waxed and waned throughout the delay. Fuentemilla et al. (2010) also observed that, during a delay period, decodable representations of memorized images recurred at a theta rhythm. More recently, single-trial analyses of monkey electrophysiological recordings in a working memory task have confirmed the absence of any continuous activity and instead identified the presence of discrete gamma bursts, paired with a decrease in beta-burst probability (Lundqvist et al., 2016). Such periodic refreshing of otherwise activity-silent representations could potentially serve as the neural correlate of conscious rehearsal, a central feature of working memory according to Baddeley (2003). It also suggests, however, that even consciously perceived

items may not always be “in mind.” Future research might attempt to more directly simulate activity-silent mechanisms in the context of conscious and non-conscious perception by, for example, relying on more elaborate models capturing decreases in alpha/beta (Lundqvist et al., 2011).

In conjunction with prior evidence (King et al., 2016; Salti et al., 2015), our findings therefore indicate that there may be two successive mechanisms for the short-term maintenance of conscious and non-conscious stimuli: an initial, transient period of ~1s, during which the representation is encoded by active firing with a slowly decaying amplitude, and an ensuing activity-silent maintenance via short-term changes in synaptic weights, during which activity either intermittently resurfaces (conscious case) or vanishes (non-conscious case). Such activity-silent retention need not necessarily be specific to working memory. Recent investigations have, for instance, demonstrated the existence of recognition memory for invisible cues (Chong et al., 2014; Rosenthal et al., 2016). As delay periods ranged in the order of minutes rather than seconds, persistent neural activity seems to be an unlikely candidate mechanism of maintenance. Activity-silent codes might have been at play, though they probably depended on mechanisms with longer time constants than the relatively rapidly decaying patterns of synaptic weights discussed in the context of the present experiments. Nevertheless, activity-silent representations may constitute a general mechanism for maintenance across the whole spectrum of temporal delays (from seconds over minutes/hours to days/weeks/decades), thus forming a generic property of memory.

Limitations and future perspectives

Our study presents limitations that should be addressed by future research. Due to the nature of the current investigation (a working memory task with long trials and subjectively determined variables), a relatively small number of unseen trials was acquired, thus making it

difficult to detect subtle effects. While our conclusions are supported by Bayes' Factor analyses, converging evidence from univariate and multivariate techniques, and similar results obtained with larger samples in the domain of activity-silent conscious working memory (e.g., Rose et al., 2016; Wolff et al., 2017), a number of our observations are based on null effects, and it remains a possibility that we missed some target- and/or response-related activity on the unseen trials. Future research should thus aim at replicating the present findings with larger datasets or with more sensitive techniques, such as intra-cranial recordings. In particular, it might be interesting to further probe the relationship between seen, unseen correct, and unseen incorrect targets: A specific prediction of the proposed model is that unseen correct trials should possess enough activity to modify synaptic weights in high-level cortical circuits, yet without crossing the threshold for sustained activity and consciousness ("failed ignition"). Unseen correct trials should thus share some of the processes that are found on seen trials and future research is necessary to directly test this hypothesis.

Conclusion

In contrast to a widely-held belief, our findings support the existence of genuine working memory in the absence of either conscious perception or sustained activity. Our proposal is that, following a transient encoding phase via active firing, non-conscious stimuli may be maintained by 'activity-silent' short-term changes in synaptic weights without any detectable neural activity, allowing above-chance retrieval for several seconds. Similar activity-silent codes also subserve conscious maintenance, though in this case periodic refreshing appears to stabilize the stored representations throughout the delay. Our findings thus highlight the need to refine our understanding of working memory, and to continuously challenge the limits of non-conscious processing.

Methods

Subjects

38 healthy volunteers participated in the present study (experiment 1: $N = 17$, $M_{age} = 23.3$ years, $SD_{age} = 2.8$ years, 10 men; experiment 2: $N = 21$, $M_{age} = 24.3$ years, $SD_{age} = 3.8$ years, 9 men). They gave written informed consent and received 80 or 15€ as compensation for the imaging and behavioral paradigms. Due to noisy recordings, only 13 of the 17 subjects in experiment 1 were retained for the MEG analyses. Although sample size had not specifically been estimated for our study, it thus was reasonable given typical experiments in the field.

Experimental protocol

Participants performed variations of a spatial delayed-response task, designed to assess retention of a target location under varying levels of subjective visibility (Figure 1A). Each trial began with the presentation of a central fixation cross (500ms), displayed in white ink on an otherwise black screen. In experiment 1, a faint gray target square (RGB: 89.25 89.25 89.25) was flashed for 17ms in 1 out of 20 equally spaced, invisible positions along a circle centered on fixation (radius = 200 pixels; 8 repetitions/location). Another fixation cross (17ms) preceded the display of the mask (233ms). Mask elements were composed of four individual squares (two right above and below, and two to the left and right of the target stimulus), arranged to tightly surround the target square without overlapping it. They appeared simultaneously at all possible target locations. Mask contrast was adjusted on an individual basis in a separate calibration procedure (see below). A variable delay period with constant fixation followed the mask (experiment 1: 2.5, 3.0, 3.5, or 4.0s). On 50% of the trials in experiment 1, an unmasked distractor square, randomly placed and with the same duration as the target, was presented 1.5s into the delay period.

After the delay, 20 letters – drawn from a subset of lower-case letters of the alphabet (excluded: *e, j, n, p, t, v*) – were randomly presented in the 20 positions (2.5s). Participants were asked to identify the target location by speaking the name of the letter presented at the

location. They were instructed to always provide a response, guessing if necessary. A trial ended with the presentation of the word *Vu?* (French for *seen*) in the center of the screen (2.5s), cueing participants to rate the visibility of the target on the 4-point Perceptual Awareness Scale (PAS; *1*: no experience of the target, *2*: brief glimpse, *3*: almost clear experience, *4*: clear experience; Ramsøy and Overgaard, 2004) using the index, middle, ring, or little finger of their right hand (five-button non-magnetic response box, Cambridge Research Systems Ltd., Fiber Optic Response Pad). We instructed subjects to reserve a visibility rating of *1* for those trials, for which they had absolutely no perception of the target. The target square was also replaced by a blank screen on 20% of the trials, in order to obtain an objective measure of participants' sensitivity to the presence of the target. The inter-trial interval (ITI) lasted 1s. Subjects completed a total of 200 trials of this working memory task, divided into four separate experimental blocks. They also undertook two blocks of 100 trials each of a perception-only control paradigm, identical to the working memory task in all respects except that the delay period and target localization screen were omitted, such that the presentation of the mask immediately preceded subjects' visibility ratings. Task order (perception vs. working memory) was counterbalanced across participants.

Experiment 2 was designed to investigate the impact of a conscious working memory load on non-conscious working memory. Apart from the following exceptions, it was identical to experiment 1: A screen with either 1 (low load) or 5 (high load) centrally presented digits (1.5s) – randomly drawn (without replacement) from the numbers 1 through 9 – as well as a 1s-fixation period were shown prior to the presentation of the target square. Following either a 0s- or a 4s-delay period, subjects first identified the target location by typing their responses on a standard AZERTY keyboard (4s). The French word for *numbers* (*Numéros?*) then probed participants to recall the sequence of digits in the correct order. Responses were again logged on the keyboard during a period of 4.5s. Subjects last rated

target visibility as in experiment 1 (3s). The ITI varied between 1 and 2s. Participants completed two experimental blocks of 100 trials each.

Calibration task

Prior to the experimental tasks, each participant's perceptual threshold was estimated in order to ensure roughly equal proportions of seen and unseen trials. Subjects completed 150 (experiment 1: 3 blocks) or 125 (experiment 2: 5 blocks) trials of a modified version of the working memory task (no distractor, delay duration: 2s in experiment 1 and 0s in experiment 2), during which mask contrast was either increased (following a visibility rating of *2*, *3*, or *4*) or decreased (following a visibility rating of *1*) on each target-present trial according to a double-staircase procedure. Individual perceptual thresholds to be used in the main tasks were derived by averaging the mask contrasts from the last four switches from seen to unseen (or vice versa) in each staircase.

Behavioral analyses

We analyzed our behavioral data in Matlab R2014a (MathWorks Inc., Natick, MA; code available upon request) and SPSS Statistics Version 20.0 (IBM, Armonk, NY), using repeated-measures analyses of variance (ANOVAs). Only meaningful trials without missing responses were included in any analysis. Distributions of localization responses were computed for visibility categories with at least five trials per subject. Objective working memory performance was quantified via two complementary measures. The *rate of correct responding* was defined as the proportion of trials within two positions (i.e.,+/- 36°) of the actual target location and served as an index of the amount of information that could be retained. Because 5 out of 20 locations were counted as correct, chance on this measure was 25%. The *precision* of working memory was estimated as the dispersion (standard deviation) of spatial responses. In particular, we modeled the observed distribution of responses *D(n)* as

762 a mixture of a uniform distribution (random guessing) and an unknown probability
763 distribution *d* ("true working memory"):
764
765 $$(1)\ \mathrm{D(n)} = \frac{\mathrm{p}}{\mathrm{N}} + \left(1\text{-}\mathrm{p}\right)\mathrm{d(n)}$$
766
767 where *p* refers to the probability that a given trial is responded to using random guessing; *N*
768 to the number of target locations (*N* = 20); and *n* is the deviation from the true target location.
769 We assumed that *d*(*n*) = 0 for deviations beyond a fixed limit *a* (with *a* = 2). This hypothesis
770 allowed us to estimate *p* from the mean of that part of the distribution *D* for which one may
771 safely assume no contribution of working memory:
772
773 $$(2)\ \hat{\mathrm{p}} = \frac{\sum \mathrm{D(n)} |\ \mathrm{n\ outside\ [-a,\ a]}}{\left(\mathrm{N\text{-}2a\text{-}1}\right)} * \mathrm{N}$$
774
775 where the model is designed in such a way as to ensure that $\hat{p} = 1$ if *D* is a uniform
776 distribution (i.e., 100% of random guessing) and $\hat{p} = 0$ if *D* vanishes outside the region of
777 correct responding (i.e., 0% of random guessing). There needs to be at least chance
778 performance inside the region of correct responding, so
779
780 $$(3)\ \sum \mathrm{D(n)} \mid \mathrm{n} \in [-\mathrm{a},\ \mathrm{a}] \geq \frac{2\mathrm{a}\text{-}1}{\mathrm{N}}$$
781
782 which ensures $0 \leq \hat{p} \leq 1$. This is the reason why, when computing precision, we included
783 only subjects whose rate of correct responding for unseen trials, collapsed across all
784 experimental conditions, significantly exceeded chance performance (i.e., 25%) in a χ^2-test (p
785 < .05). An estimate of *d*, $\hat{d}$, can then be derived in two steps from Equation 1 as

$$(4)\ \delta(n) = \frac{D(n) - \frac{\hat{p}}{N}}{1 - \hat{p}}$$

$$(5)\ \hat{d}(n) = \frac{\delta(n)|n\in[-a, a]}{\sum \delta(n)|n\in[-a, a]}.$$

We note that the distribution δ has residual, yet negligible, positive and negative mass (due to noise) outside the region of correct responding. In order to obtain $\hat{d}$, we therefore restricted the distribution δ to [-*a*, *a*], set all negative values to 0, and renormalized its mass to 1. The precision of the representation of the target location in working memory was then defined as the standard deviation of that distribution.

MEG recordings and preprocessing

In experiment 1, we recorded MEG with a 306-channel (102 sensor triplets: 1 magnetometer and 2 orthogonal planar gradiometers), whole-head setup by ElektaNeuromag® (Helsinki, Finland) at 1000Hz with a hardware bandpass filter between 0.1 and 330Hz. Eye movements as well as heart rate were monitored with vertical and horizontal EOG and ECG channels. Prior to installation of the subject in the MEG chamber, we digitized three head landmarks (nasion and pre-auricular points), four head position indicator (HPI) coils placed over frontal and mastoïdian skull areas, and 60 additional locations outlining the participant's head with a 3-dimensional Fastrak system (Polhemus, USA). Head position was measured at the beginning of each run.

Our preprocessing pipeline followed Marti et al. (2015). Using MaxFilter Software (ElektaNeuromag®, Helsinki, Finland), raw MEG signals were first cleaned of head movements, bad channels, and magnetic interference originating from outside the MEG helmet (Taulu et al., 2004), and then downsampled to 250Hz. We conducted all further preprocessing steps with the Fieldtrip toolbox (http://www.fieldtriptoolbox.org/; Oostenveld

et al., 2011) run in a Matlab R2014a environment. Initially, MEG data were epoched between -0.5 and +2.5s with respect to target onset for all stimulus-locked, and between -0.5 and +0.8s with respect to the onset of the response screen for all response-locked analyses. Trials contaminated by muscle or other movement artifacts were then identified and rejected in a semi-automated procedure, for which the variance of the MEG signals across sensors served as an index of contamination. To remove any residual eye-movement and cardiac artifacts, we performed independent component analysis separately for each channel type, visually inspected the topographies and time courses of the first 30 components, and subtracted any contaminated component from the MEG data. Except for analyses requiring higher spatial precision (i.e., circular-linear correlations and decoding), results are presented for magnetometers only.

Further preprocessing steps depended on the nature of the subsequent analysis: Epochs retained for investigations based on evoked responses (i.e., ERFs, decoding, circular-linear correlations) were low-pass filtered at 30Hz, while time-frequency decompositions relied on entirely unfiltered data. In the latter case, a sliding, frequency-independent Hann taper (window size: 500ms, step size: 20ms) was convolved with the unfiltered epochs in order to extract an estimate of power between 1 and 99Hz (in 2Hz steps) to identify the neural correlates of conscious and non-conscious perception and working memory in the frequency domain. Prior to univariate or multivariate statistical analysis, data (ERFs, time-frequency power estimates) were baseline corrected using a period between -200 and -50ms.

Circular-linear correlations

To localize and track the neural representations of target, response, and distractor location, filtered epochs were transformed into circular-linear correlation coefficients. Following King et al. (2016), we combined the two linear correlation coefficients between the MEG signal and the sine and cosine of the angle defining the location in question (i.e., target,

distractor, or response). An empirical null distribution was generated for each condition separately by shuffling the labels (i.e., target, distractor, or response location) at the corresponding time points and averaging the resulting distribution from 1000 such permutations.

Due to the spatial nature of our task, there is a possibility that subjects could have systematically moved their eyes after the presentation of the target, thus contaminating the correlation analyses. However, several lines of evidence suggest that this was not the case: First, participants were carefully instructed not to move their eyes. A close inspection of the EOG traces confirmed that subjects successfully implemented this request and did not display any strategic eye movements. Second, we carefully removed any trials contaminated by such movements as part of our preprocessing procedure. Third, the topographical patterns of the correlations show that the signal primarily originated in occipital and parietal channels. Eye movements therefore unlikely have driven the circular-linear correlations.

Sources

Individual anatomical magnetic resonance images (MRI), obtained with a 3D T1-weighted spoiled gradient recalled pulse sequence (voxel size: 1 * 1 * 1.1mm; repetition time [TR]: 2,300ms; echo time [TE]: 2.98ms; field of view [FOV]: 256 * 240 * 176mm; 160 slices) in a 3T Tim Trio Siemens scanner, were first segmented into gray/white matter as well as subcortical structures with FreeSurfer (https://surfer.nmr.mgh.harvard.edu/). We then reconstructed the cortical, scalp, and head surfaces in Brainstorm (http://neuroimage.usc.edu/brainstorm; Tadel et al., 2011) and co-registered these anatomical images with the MEG signals, using the HPI coils and the digitized head shape as a reference. Current density distributions on the cortical surface were subsequently estimated separately for each condition and subject. Specifically, we employed an analytical model with overlapping spheres to compute the leadfield matrix and modeled neuronal current sources

with an unconstrained (dipole orientation loosening factor: 0.2) weighted minimum-norm current estimate (wMNE; depth-weighting factor: 0.5) and a noise covariance obtained from the baseline period of all trials. Average time-frequency power in the alpha (8 – 12Hz) and beta (13 – 30 Hz) band was then estimated with complex Morlet wavelets using the Brainstorm default parameters, the resulting transformations projected onto the ICBM 152 anatomical template (Fonov et al., 2011, 2009), and the contrasts between the conditions of interest computed. Group averages for spatial clusters of at least 150 vertices are shown in dB relative to baseline and were thresholded at 60% of the maximum amplitude (cortex smoothed at 60%).

Multivariate pattern analyses

We employed the Scikit-Learn package (Pedregosa et al., 2011) as implemented in MNE 0.13 (Gramfort, 2013; Gramfort et al., 2014) in order to conduct our multivariate pattern analyses (MVPA). Following Marti et al. (2015) and King et al. (2016), we fit linear estimators at each time sample within each participant to isolate the topographical patterns best differentiating our experimental conditions. Support vector machines (Chang and Lin, 2011) were trained in the case of categorical data (i.e., visibility/accuracy) and a combination of two linear support vector regressions was used for circular data (i.e., target/response location) to estimate an angle from the arctangent of the separately predicted sine and cosine of the labels of interest.

A 5- (for categorical variables) or, due to the much larger number of labels, 2-fold (for circular variables), stratified cross-validation procedure was used in order to avoid overfitting: MEG data were first split into five (two) sets of trials with the same proportion of samples for each class. Within each fold, four (one) of these sets served as the training data and the remainder as the testing data. Model fitting, including all preprocessing steps, was exclusively performed on the training set. 50% of the most informative features (i.e., channels) were

selected by means of a simple, univariate analysis of variance to reduce the dimensionality of the data (Charles et al., 2014; Haynes and Rees, 2006), the remaining channel-time features *z*-score normalized, and a weighting procedure applied in order to counteract the effects of any class imbalances. The classifier was then trained on the resulting data and applied to the left-out trials in order to identify the hyperplane (i.e., topography) best suited to separate the classes. This sequence of events (univariate feature selection, normalization, training and testing) was repeated five (two) times, ensuring that each trial would be included in the test set once.

Within the same cross-validation loop, we also evaluated the ability of each classifier to discriminate the experimental conditions of interest at all other time samples (i.e., generalization across time). This kind of MVPA results in a temporal generalization matrix, in which each entry represents the decoding performance of each classifier trained at time point *t* and tested at time point *t'*, and in which the diagonal corresponds to classifiers trained and tested on the same time points (King and Dehaene, 2014). Importantly, when interrogating the capacity of our classifiers to generalize across tasks or labels (e.g., from the perception to the working memory task, or from seen to unseen correct target locations), we modified the aforementioned cross-validation procedure to capitalize on the independence of our training and testing data (see http://martinos.org/mne/dev/auto_examples/decoding/plot_decoding_time_generalization_conditions.html#example-decoding-plot-decoding-time-generalization-conditions-py). As such, classifiers from each training set were directly applied to the entire testing set and the respective predictions averaged.

Classifiers for categorical data generated a continuous output in the form of the distance between the respective sample and the separating hyperplane for each test trial. In order to be able to compare classification performance across subjects, we then applied a

receiver operating characteristic analysis across trials within each participant and summarized overall effect sizes with the area under the curve (AUC). Unlike average decoding accuracy, the AUC serves as an unbiased measure of decoding performance as it represents the true-positive rate (e.g., a trial was correctly categorized as seen) as a function of the false-positive rate (e.g., a trial was incorrectly categorized as seen). Chance performance, corresponding to equal proportions of true and false positives, therefore leads to an AUC of 0.5. Any value greater than this critical level implies better-than-chance performance, with an AUC of 1 indicating a perfect prediction for any given class. In contrast, classifiers for circular data were first summarized by computing the mean absolute difference between the predicted and the actual angle (range: 0 to π; chance: $\pi/2$) and then transformed into an "accuracy" score (range: $-\pi/2$ to $\pi/2$; chance: 0). To facilitate comparability between different conditions, an additional baseline-correction was then performed.

Statistical analyses

We performed statistical analyses across subjects. For the ERF and time-frequency data, cluster-based, non-parametric *t*-tests with Monte Carlo permutations were used to identify significant differences between experimental conditions (Maris and Oostenveld, 2007). Further planned comparisons of ERF time courses (seen vs. unseen) in a-priori defined spatio-temporal regions of interest (i.e., P3b time window: 300 – 600ms) were conducted with non-parametric signed-rank tests ($p_{\text{uncorrected}} < .05$). A correction for multiple comparisons was then applied with a false discovery rate ($p_{\text{FDR}} < .05$).

Non-parametric signed-rank tests ($p_{\text{uncorrected}} < .05$) were also employed to evaluate decoding performance and the strength of circular-linear correlations. Specifically, we assessed whether classifiers could predict the trials' classes better than chance (categorical data: AUC > 0.5; circular data: rad > 0) and whether circular-linear correlation coefficients deviated from an empirical baseline (Δ rho > 0). We report temporal averages over four a-

priori time bins, corresponding to an early perceptual period (0.1 – 0.3s), the P3b time window (0.3 – 0.6s), and the first (0.6 – 1.55s) and second (1.55 – 2.53s) part of the delay period. To capitalize on the increased spatial selectivity of gradiometers, averaged time courses of these two channels are shown for circular-linear correlations.

Bayesian statistics, based on either two- (time-frequency analyses) or one-sided (circular-linear correlations) *t*-tests, were also computed when appropriate with a scale factor of $r = .707$ (Rouder et al., 2009).

Simulations

A one-dimensional, recurrent continuous attractor neural network (CANN) model (Mongillo et al., 2008) was adapted in order to simulate the experimental findings (Figure 7A). Individual neurons were aligned according to their preferred stimulus value, enabling the network to encode angular position of a target stimulus (range: $-\pi$ to π; periodic boundary condition). The dynamics of this system were determined by the synaptic currents of each neuron given by

$$(6)\ \tau\frac{\partial h_E(\theta, t)}{\partial t} = -h_\theta+\rho\int_{-\pi}^{\pi} J(\theta, \theta')u(\theta', t)x(\theta', t)R_E(\theta', t)d\theta'-J_{EI}R_I+I_b+\delta_1\xi_1(\theta, t)+I_e+\delta_2\xi_2(\theta, t),$$

$$(7)\ \frac{\partial u(\theta, t)}{\partial t}= \frac{U-u(\theta, t)}{\tau_f}+U\left[1-u(\theta, t)\right]R_E(\theta, t),$$

$$(8)\ \frac{\partial x(\theta ,t)}{\partial t} = \frac{1-x(\theta, t)}{\tau_d}-u(\theta, t)x(\theta, t)R_E(\theta, t), \text{ and}$$

$$(9)\ \tau\frac{\partial h_I}{\partial t} = -h_I+J_{IE}\int_{-\pi}^{\pi} R_E(\theta, t)\,,$$

where τ describes the time constant of firing rate dynamics (in the order of milliseconds); ρ refers to neuronal density; $h_E(\theta,t)$ and $R_E(\theta,t)$ capture the synaptic current to and firing rate of neurons with preference θ at time t respectively; and $R(h) = \alpha \ln(1 + \exp(h/\alpha))$ is the neural gain chosen in the form of a smoothed threshold-linear function. J_{IE} and J_{EI} represent the

connection strength between excitatory and inhibitory neurons. All excitatory neurons received a constant background input, I_e, reflecting the arousal signal when the neural system was engaged in a working memory task. $\delta_1\xi_1$ is background noise; I_e, any external stimulus (e.g., target, mask, and recall signal); and $\delta_1\xi_1$ (t) the noise related to those external stimuli. u (θ, t) and x (θ, t) denote the short-term synaptic facilitation (STF) and depression (STD) effects at time t of neurons with preference θ, respectively. The short-term plasticity dynamics are characterized by the following parameters: J_1 (absolute efficacy), U (increment of the release probability when a spike arrives), τ_f and τ_d (facilitation and depression time constants). The STF value u (θ, t) is facilitated whenever a spike arrives, and decays to the baseline U within the time τ_f. The neurotransmitter value x (θ, t) is utilized by each spike in proportion to u (θ, t) and then recovers to its baseline, 1, within the time τ_d.

J (θ, θ') is the interaction strength from neurons at θ to neurons at θ' and is chosen to be

$$(10)\ J(\theta, \theta') = \begin{cases} J_1 \cos\left[B * (\theta - \theta')\right] - J_0, & \text{if } B * (\theta - \theta') \in [-\arccos(-J_0/J_1), \arccos(-J_0/J_1)], \\ -J_0, & \text{else} \end{cases}$$

where J_0, J_1, and B are constants which determine the connection strength between the neurons. Note that J (θ, θ') is a function of $\theta - \theta'$, i. e., the neuronal interactions are translation-invariant in the space of neural preferred stimuli. The other parameters of the system were as follows: $\tau = 0.008$s, $\tau_f = 4$s, $\tau_d = 0.3$s, $J_1 = 12$, $J_0 = 1$, $J_{EI} = 1.9$, $J_{IE} = 1.8$, $I_b = -0.1$Hz, $\delta_1 = 0.3$, $\delta_2 = 9$, $N = 100$, $\alpha = 1.5$, $B = 2.2$.

During our simulations, we first presented a target signal with an amplitude of $A_{\text{target}} = 390$Hz at a random location (50ms), waited for 17ms, and then applied a mask signal to all the neurons in the system (200ms). The amplitude of the mask signal was initially varied in order

to determine a critical value which would produce two distinct maintenance patterns, but was then fixed at a threshold of A_{mask} = 62Hz. At the end of a 3s-delay period, a non-specific recall signal was given for 50ms with A_{recall} = 10Hz. Remembered target position was calculated as the population vector angle during this time period.

Figure Supplements

Figure 2 – Supplement 1. Perceptual sensitivity does not correlate with working memory performance on unseen trials.

Figure 4 – Supplement 1. Alpha- and beta-band desynchronizations serve as a general signature of conscious processing and conscious working memory.

Figure 4 – Supplement 2. Seen and unseen correct trials do not share the same discriminative decoding axis.

Figure 4 – Supplement 3. Bayesian statistics for the time-frequency analyses.

Figure 5 – Supplement 1. Representation of seen target locations during conscious perception and working memory.

Figure 5 – Supplement 2. Circular-linear correlations and multivariate decoding reveal similar time courses for target location.

Figure 5 – Supplement 3. Tracking target/response location on unseen correct and incorrect trials with multivariate decoding.

Figure 6 – Supplement 1. Topographies for circular-linear correlations with response location as a function of visibility.

Figure 6 – Supplement 2. Circular-linear correlations and multivariate decoding reveal similar time courses for response location.

Acknowledgements

We gratefully acknowledge Henrik Ueberschär, Leila Azizi, and Virginie Van Wassenhove for their invaluable daily support and stimulating discussion.

Competing Interests

The authors declare no competing interests.

References

Baars, B.J., Franklin, S., 2003. How conscious experience and working memory interact. Trends Cogn. Sci. 7, 166–172. doi:10.1016/S1364-6613(03)00056-1

Baddeley, A., 2003. Working memory: looking back and looking forward. Nat. Rev. Neurosci. 4, 829–839. doi:10.1038/nrn1201

Bergström, F., Eriksson, J., 2014. Maintenance of non-consciously presented information engages the prefrontal cortex. Front. Hum. Neurosci. 8. doi:10.3389/fnhum.2014.00938

Bergström, F., Eriksson, J., 2015. The conjunction of non-consciously perceived object identity and spatial position can be retained during a visual short-term memory task. Front. Psychol. 6. doi:10.3389/fpsyg.2015.01470

Chang, C.-C., Lin, C.-J., 2011. LIBSVM: A library for support vector machines. ACM Trans. Intell. Syst. Technol. 2, 1–27. doi:10.1145/1961189.1961199

Charles, L., King, J.-R., Dehaene, S., 2014. Decoding the Dynamics of Action, Intention, and Error Detection for Conscious and Subliminal Stimuli. J. Neurosci. 34, 1158–1170. doi:10.1523/JNEUROSCI.2465-13.2014

Chaudhuri, R., Bernacchia, A., Wang, X.-J., 2014. A diversity of localized timescales in network activity. eLife 3. doi:10.7554/eLife.01239

Chong, T.T.-J., Husain, M., Rosenthal, C.R., 2014. Recognizing the unconscious. Curr. Biol. 24, R1033–R1035. doi:10.1016/j.cub.2014.09.035

Cooper, N.R., Croft, R.J., Dominey, S.J.., Burgess, A.P., Gruzelier, J.H., 2003. Paradox lost? Exploring the role of alpha oscillations during externally vs. internally directed attention and the implications for idling and inhibition hypotheses. Int. J. Psychophysiol. 47, 65–74. doi:10.1016/S0167-8760(02)00107-1

Dehaene, S., Changeux, J.-P., 2011. Experimental and Theoretical Approaches to Conscious Processing. Neuron 70, 200–227. doi:10.1016/j.neuron.2011.03.018

Dehaene, S., Charles, L., King, J.-R., Marti, S., 2014. Toward a computational theory of conscious processing. Curr. Opin. Neurobiol. 25, 76–84. doi:10.1016/j.conb.2013.12.005

Dehaene, S., Naccache, L., 2001. Towards a cognitive neuroscience of consciousness: basic evidence and a workspace framework. Cognition 79, 1–37.

Del Cul, A., Baillet, S., Dehaene, S., 2007. Brain Dynamics Underlying the Nonlinear Threshold for Access to Consciousness. PLoS Biol. 5, e260. doi:10.1371/journal.pbio.0050260

Dupoux, E., Gardelle, V. de, Kouider, S., 2008. Subliminal speech perception and auditory streaming. Cognition 109, 267–273. doi:10.1016/j.cognition.2008.06.012

Dutta, A., Shah, K., Silvanto, J., Soto, D., 2014. Neural basis of non-conscious visual working memory. NeuroImage 91, 336–343. doi:10.1016/j.neuroimage.2014.01.016

Eriksson, J., Vogel, E.K., Lansner, A., Bergström, F., Nyberg, L., 2015. Neurocognitive Architecture of Working Memory. Neuron 88, 33–46. doi:10.1016/j.neuron.2015.09.020

Fonov, V., Evans, A.C., Botteron, K., Almli, C.R., McKinstry, R.C., Collins, D.L., 2011. Unbiased average age-appropriate atlases for pediatric studies. NeuroImage 54, 313–327. doi:10.1016/j.neuroimage.2010.07.033

Fonov, V., Evans, A., McKinstry, R., Almli, C., Collins, D., 2009. Unbiased nonlinear average age-appropriate brain templates from birth to adulthood. NeuroImage 47, S102. doi:10.1016/S1053-8119(09)70884-5

Fuentemilla, L., Penny, W.D., Cashdollar, N., Bunzeck, N., Düzel, E., 2010. Theta-Coupled Periodic Replay in Working Memory. Curr. Biol. 20, 606–612. doi:10.1016/j.cub.2010.01.057

Fujisawa, S., Amarasingham, A., Harrison, M.T., Buzsáki, G., 2008. Behavior-dependent short-term assembly dynamics in the medial prefrontal cortex. Nat. Neurosci. 11, 823–833. doi:10.1038/nn.2134

Gaillard, R., Dehaene, S., Adam, C., Clémenceau, S., Hasboun, D., Baulac, M., Cohen, L., Naccache, L., 2009. Converging Intracranial Markers of Conscious Access. PLoS Biol. 7, e1000061. doi:10.1371/journal.pbio.1000061

Gramfort, A., 2013. MEG and EEG data analysis with MNE-Python. Front. Neurosci. 7. doi:10.3389/fnins.2013.00267

Gramfort, A., Luessi, M., Larson, E., Engemann, D.A., Strohmeier, D., Brodbeck, C., Parkkonen, L., Hämäläinen, M.S., 2014. MNE software for processing MEG and EEG data. NeuroImage 86, 446–460. doi:10.1016/j.neuroimage.2013.10.027

Greenwald, A.G., Draine, S.C., Abrams, R.L., 1996. Three cognitive markers of unconscious semantic activation. Science 273, 1699–1702.

Gross, J., Schnitzler, A., Timmermann, L., Ploner, M., 2007. Gamma Oscillations in Human Primary Somatosensory Cortex Reflect Pain Perception. PLoS Biol. 5, e133. doi:10.1371/journal.pbio.0050133

Harrison, S.A., Tong, F., 2009. Decoding reveals the contents of visual working memory in early visual areas. Nature 458, 632–635. doi:10.1038/nature07832

Haynes, J.-D., Rees, G., 2006. Decoding mental states from brain activity in humans. Nat. Rev. Neurosci. 7, 523–534. doi:10.1038/nrn1931

Jensen, O., Mazaheri, A., 2010. Shaping Functional Architecture by Oscillatory Alpha Activity: Gating by Inhibition. Front. Hum. Neurosci. 4. doi:10.3389/fnhum.2010.00186

King, J.-R., Pescetelli, N., Dehaene, S., 2016. Brain mechanisms underlying the brief maintenance of seen and unseen sensory information. Neuron. 92, 1122–1134. doi: 10.1016/j.neuron.2016.10.051

King, J.-R., Dehaene, S., 2014. Characterizing the dynamics of mental representations: the temporal generalization method. Trends Cogn. Sci. 18, 203–210. doi:10.1016/j.tics.2014.01.002

King, J.-R., Gramfort, A., Schurger, A., Naccache, L., Dehaene, S., 2014. Two Distinct Dynamic Modes Subtend the Detection of Unexpected Sounds. PLoS ONE 9, e85791. doi:10.1371/journal.pone.0085791

Lamme, V.A.F., Roelfsema, P.R., 2000. The distinct modes of vision offered by feedforward and recurrent processing. Trends Neurosci. 23, 571–579. doi:10.1016/S0166-2236(00)01657-X

Lundqvist, M., Herman, P., Lansner, A., 2011. Theta and gamma power increases and alpha/beta power decreases with memory load in an attractor network model. J. Cogn. Neurosci. 23, 3008–3020. doi:10.1162/jocn_a_00029

Lundqvist, M., Rose, J., Herman, P., Brincat, S.L., Buschman, T.J., Miller, E.K., 2016. Gamma and Beta Bursts Underlie Working Memory. Neuron 90, 152–164. doi:10.1016/j.neuron.2016.02.028

Maris, E., Oostenveld, R., 2007. Nonparametric statistical testing of EEG- and MEG-data. J. Neurosci. Methods 164, 177–190. doi:10.1016/j.jneumeth.2007.03.024

Marti, S., King, J.-R., Dehaene, S., 2015. Time-Resolved Decoding of Two Processing Chains during Dual-Task Interference. Neuron 88, 1297–1307. doi:10.1016/j.neuron.2015.10.040

Merikle, P., 2001. Perception without awareness: perspectives from cognitive psychology. Cognition 79, 115–134. doi:10.1016/S0010-0277(00)00126-8

Mongillo, G., Barak, O., Tsodyks, M., 2008. Synaptic Theory of Working Memory. Science 319, 1543–1546. doi:10.1126/science.1150769

Naghavi, H.R., Nyberg, L., 2005. Common fronto-parietal activity in attention, memory, and consciousness: Shared demands on integration? Conscious. Cogn. 14, 390–425. doi:10.1016/j.concog.2004.10.003

Oberauer, K., 2002. Access to information in working memory: Exploring the focus of attention. J. Exp. Psychol. Learn. Mem. Cogn. 28, 411–421. doi:10.1037//0278-7393.28.3.411

Oostenveld, R., Fries, P., Maris, E., Schoffelen, J.-M., 2011. FieldTrip: Open Source Software for Advanced Analysis of MEG, EEG, and Invasive Electrophysiological Data. Comput. Intell. Neurosci. 2011, 1–9. doi:10.1155/2011/156869

Pedregosa, Fabian, Varoquaux, Gael, Gramfort, Alexandre, Michel, Vincent, Thirion, Bertrand, Grisel, Olivier, Blondel, Mathieu, Prettenhofer, Peter, Weiss, Ron, Dubourg, Vincent, Vanderplas, Jake, Passos, ALexandre, Cournapeau, David, Brucher, Matthieu, Perrot, Matthieu, Duchesnay, Edouard, 2011. Scikit-learn: Machine Learning in Python. J. Mach. Learn. Res. 2825–2830.

Ramsøy, T.Z., Overgaard, M., 2004. Introspection and subliminal perception. Phenomenol. Cogn. Sci. 3, 1–23. doi:10.1023/B:PHEN.0000041900.30172.e8

Roelfsema, P.R., 2015. The role of the different layers of primary visual cortex in working memory. J. Vis. 15, 1406. doi:10.1167/15.12.1406

Rose, N.S., LaRocque, J.J., Riggall, A.C., Gosseries, O., Starrett, M.J., Meyering, E.E., Postle, B.R., 2016. Reactivation of latent working memories with transcranial magnetic stimulation. Science 354, 1136–1139. doi:10.1126/science.aah7011

Rosenthal, C.R., Andrews, S.K., Antoniades, C.A., Kennard, C., Soto, D., 2016. Learning and Recognition of a Non-conscious Sequence of Events in Human Primary Visual Cortex. Curr. Biol. 26, 834–841. doi:10.1016/j.cub.2016.01.040

Rouder, J.N., Speckman, P.L., Sun, D., Morey, R.D., Iverson, G., 2009. Bayesian t tests for accepting and rejecting the null hypothesis. Psychon. Bull. Rev. 16, 225–237. doi:10.3758/PBR.16.2.225

Salti, M., Monto, S., Charles, L., King, J.-R., Parkkonen, L., Dehaene, S., 2015. Distinct cortical codes and temporal dynamics for conscious and unconscious percepts. eLife 4. doi:10.7554/eLife.05652

Schurger, A., Sarigiannidis, I., Naccache, L., Sitt, J.D., Dehaene, S., 2015. Cortical activity is more stable when sensory stimuli are consciously perceived. Proc. Natl. Acad. Sci. 112, E2083–E2092. doi:10.1073/pnas.1418730112

Sergent, C., Baillet, S., Dehaene, S., 2005. Timing of the brain events underlying access to consciousness during the attentional blink. Nat. Neurosci. 8, 1391–1400. doi:10.1038/nn1549

Soto, D., Mäntylä, T., Silvanto, J., 2011. Working memory without consciousness. Curr. Biol. 21, R912–R913. doi:10.1016/j.cub.2011.09.049

Soto, D., Silvanto, J., 2014. Reappraising the relationship between working memory and conscious awareness. Trends Cogn. Sci. 18, 520–525. doi:10.1016/j.tics.2014.06.005

Sprague, T.C., Ester, E.F., Serences, J.T., 2016. Restoring Latent Visual Working Memory Representations in Human Cortex. Neuron 91, 694–707. doi:10.1016/j.neuron.2016.07.006

Stein, T., Kaiser, D., Hesselmann, G., 2016. Can working memory be non-conscious? Neurosci. Conscious. 2016, niv011. doi:10.1093/nc/niv011
Stokes, M.G., 2015. "Activity-silent" working memory in prefrontal cortex: a dynamic coding framework. Trends Cogn. Sci. 19, 394–405. doi:10.1016/j.tics.2015.05.004
Stokes, M.G., Wolff, M.J., Spaak, E., 2015. Decoding Rich Spatial Information with High Temporal Resolution. Trends Cogn. Sci. 19, 636–638. doi:10.1016/j.tics.2015.08.016
Tadel, F., Baillet, S., Mosher, J.C., Pantazis, D., Leahy, R.M., 2011. Brainstorm: A User-Friendly Application for MEG/EEG Analysis. Comput. Intell. Neurosci. 2011, 1–13. doi:10.1155/2011/879716
Taulu, S., Kajola, M., Simola, J., 2004. Suppression of interference and artifacts by the Signal Space Separation Method. Brain Topogr. 16, 269–275.
Tononi, G., Koch, C., 2008. The Neural Correlates of Consciousness: An Update. Ann. N. Y. Acad. Sci. 1124, 239–261. doi:10.1196/annals.1440.004
van Gaal, S., Lamme, V.A.F., 2012. Unconscious High-Level Information Processing: Implication for Neurobiological Theories of Consciousness. The Neuroscientist 18, 287–301. doi:10.1177/1073858411404079
Wolff, M.J., Ding, J., Myers, N.E., Stokes, M.G., 2015. Revealing hidden states in visual working memory using electroencephalography. Front. Syst. Neurosci. 9. doi:10.3389/fnsys.2015.00123
Wolff, M.J., Jochim, J., Akyürek, E.G., Stokes, M.G., 2017. Dynamic hidden states underlying working-memory-guided behavior. Nat. Neurosci. 20, 864–871. doi:10.1038/nn.4546
Wyart, V., Tallon-Baudry, C., 2009. How Ongoing Fluctuations in Human Visual Cortex Predict Perceptual Awareness: Baseline Shift versus Decision Bias. J. Neurosci. 29, 8715–8725. doi:10.1523/JNEUROSCI.0962-09.2009

Figure Legends

Figure 1. General experimental design and behavioral performance in the working memory task

(A) Experimental design. A subsequently masked target square was flashed in 1 out of 20 positions. Subjects were asked to report this location after a delay of up to 4s and to rate the visibility of the target on a 4-point scale. A visible distractor square with features otherwise identical to the target was shown on 50% of the trials during the retention period (at 1.75s). In a perception-only control condition, the maintenance phase and location response were omitted, and subjects assessed the visibility of the target immediately after the mask. **(B)** Spatial distributions of forced-choice localization performance in the working memory task (experiment 1; 0 = correct target location; positive = clockwise offset). Error bars indicate standard error of the mean (SEM) across subjects. The horizontal, dotted line illustrates chance-level at 5%. Percentages show proportion of target-present trials from a given visibility category. Due to low number of trials in individual visibility ratings *2*, *3*, and *4*, all *seen* categories were collapsed for analyses.

Figure 2. Behavioral evidence for non-conscious working memory

Spatial distributions of responses (0 = correct target location; positive = clockwise offset) as a function of visibility and distractor presence **(A)**, conscious working memory load **(B)** and delay duration **(C)**. Insets show rate of correct responding (within +/- 2 positions of actual location) and precision of working memory representation separately for seen and unseen trials. Error bars represent standard error of the mean (SEM) across subjects and horizontal, dotted line indicates chance-level (5%). *$p < .05$, **$p < .01$, and ***$p < .001$ in a paired sample *t*-test. Del = delay, Dis = distractor, L = load.

The following figure supplement is available for Figure 2:

Figure 2 – Supplement 1. Perceptual sensitivity does not correlate with working memory performance on unseen trials.

Figure 3. Neural signatures for conscious perception and maintenance in working memory

(A) Sequence of brain activations (-200 – 800ms) evoked by consciously perceiving the target in the perception (top) and working memory (bottom) task. Each topography depicts the difference in amplitude between seen and unseen trials over a 100ms time window centered on the time points shown (magnetometers only).

(B) Average time courses of seen and unseen trials (-200 – 800ms) after subtraction of target-absent trials in a group of parietal magnetometers in the perception (left) and working memory (right) task. Shaded area illustrates standard error of the mean (SEM) across subjects. Significant differences between conditions are depicted with a horizontal, black line (Wilcoxon signed-rank test across subjects, uncorrected). For display purposes, data were lowpass-filtered at 8Hz. T = target onset.

(C) Temporal generalization matrices for decoding of visibility category as a function of training and testing task. In each panel, a classifier was trained at every time sample (y-axis) and tested on all other time points (x-axis). The diagonal gray line demarks classifiers trained and tested on the same time sample. Please note the event markers in any panel involving the perception task: Mean reaction time (target-present trials) for the visibility response is indicated as vertical and/or horizontal, dotted lines. Any classifier beyond this point only reflects post-visibility processes. Time courses of diagonal decoding and of classifiers averaged over the P3b time window (0.3 – 0.6s) and over the working memory maintenance period (0.8 – 2.5s) are shown as black, red, and blue insets. Thick lines indicate significant, above-chance decoding of visibility (Wilcoxon signed-rank test across subjects, uncorrected,

two-tailed except for diagonal). For display purposes, data were smoothed using a moving average with a window of eight samples. AUC = area under the curve.

Figure 4. A sustained decrease in alpha/beta power as a marker of conscious working memory

(A) Average time-frequency power relative to baseline (dB) as a function of task and visibility category in a group of occipital (left) and fronto-central (right) magnetometers. Mean reaction time (target-present trials) for the visibility response in the perception task is indicated as a vertical, dotted line.

(B) Beta band activity (13 – 30Hz; 0 – 2.1s) related to conscious working memory (seen – unseen trials) as shown in magnetometers (top) and source space (bottom; in dB relative to baseline). Black asterisks indicate sensors showing a significant difference as assessed by a Monte-Carlo permutation test.

(C) Same as in (A) and (B) but for unseen correct and unseen incorrect trials in the alpha band (8 – 12Hz).

The following figure supplement is available for Figure 4:

Figure 4 – Supplement 1. Alpha- and beta-band desynchronizations serve as a general signature of conscious processing and conscious working memory.

Figure 4 – Supplement 2. Seen and unseen correct trials do not share the same discriminative decoding axis.

Figure 4 – Supplement 3. Bayesian statistics for the time-frequency analyses.

Figure 5. Tracking the contents of conscious and non-conscious working memory

(A) Topographies (top) and time courses (bottom; -0.2 – 2.5s) of average circular-linear correlations between the amplitude of the MEG signal (gradiometers) and target/distractor

location. Shaded area demarks standard error of the mean (SEM) across subjects. Thick line represents significant increase in correlation coefficient as compared to an empirical baseline (one-tailed Wilcoxon signed-rank test across subjects, uncorrected).

(B) Average time courses (-0.2 – 2.5s) of circular-linear correlation coefficients between amplitude of the ERFs and target location as a function of visibility in the working memory task in a group of left temporo-occipital (left), occipital (middle), and right temporo-occipital (right) gradiometers. Shaded area demarks standard error of the mean (SEM) across subjects. Thick line represents significant increase in correlation coefficient as compared to an empirical baseline (one-tailed Wilcoxon signed-rank test across subjects, uncorrected). Insets show average correlation coefficients (relative to an empirical baseline) over four time windows: 0.1 – 0.3s (early), 0.3 – 0.6s (P3b), 0.6 – 1.55s (Del1), and 1.55 – 2.5s (Del2). White asterisks denote significant differences to baseline (one-tailed Wilcoxon signed-rank test across subjects), black asterisks significant differences between conditions (two-tailed Wilcoxon signed-rank test across subjects). For display purposes, data were lowpass-filtered at 8Hz. *$p < .05$, **$p < .01$, and ***$p < .001$. Del1= first part of delay, Del2 = second part of delay, T = target onset.

(C) Same as in (B), but as a function of accuracy on the unseen trials (correct = within +/-2 positions of the target).

The following figure supplement is available for Figure 5:

Figure 5 – Supplement 1. Representation of seen target locations during conscious perception and working memory.

Figure 5 – Supplement 2. Circular-linear correlations and multivariate decoding reveal similar time courses for target location.

Figure 5 – Supplement 3. Tracking target/response location on unseen correct and incorrect trials with multivariate decoding.

Figure 6. Tracking response location in conscious and non-conscious working memory

(A) Topographies of average circular-linear correlations between the amplitude of the MEG signal (gradiometers) and response location. R = onset of the response screen.

(B) Average time courses (left: stimulus-locked, -0.2 – 2.5s; right: response-locked, -0.5 – 0.8s) of circular-linear correlation coefficients between amplitude of the ERFs and response location as a function of visibility in the working memory task in a group of occipital (top, left), frontal (top, right) left temporo-occipital (bottom, left) and right temporo-occipital (bottom, right) gradiometers. Shaded area demarks standard error of the mean (SEM) across subjects. Thick line represents significant increase in correlation coefficient as compared to an empirical baseline (one-tailed Wilcoxon signed-rank test across subjects, uncorrected). Insets show average correlation coefficients (relative to an empirical baseline) over four stimulus-locked time windows, 0.1 – 0.3s (early), 0.3 – 0.6s (P3b), 0.6 – 1.55s (Del1), and 1.55 – 2.5s (Del2), and two response-locked time windows, -0.5 – 0.0s (Del3) and 0.0 – 0.8s (Resp). White asterisks denote significant differences to baseline (one-tailed Wilcoxon signed-rank test across subjects), black asterisks significant differences between conditions (two-tailed Wilcoxon signed-rank test across subjects). For display purposes, data were lowpass-filtered at 8Hz. *$p < .05$, **$p < .01$, and ***$p < .001$. Del1= first part of delay, Del2 = second part of delay, Del3 = last 500ms before response screen, R = response screen onset, T = target onset.

(C) Same as in (B), but as a function of accuracy on the unseen trials (correct = within +/-2 positions of the target).

The following figure supplement is available for Figure 6:

Figure 6 – Supplement 1. Topographies for circular-linear correlations with response location as a function of visibility.

Figure 6 – Supplement 2. Circular-linear correlations and multivariate decoding reveal similar time courses for response location.

Figure 7. Activity-silent neural mechanisms underlying conscious and non-conscious working memory

(A) Structure of a one-dimensional continuous attractor neural network (CANN). Neuronal connections $J(\theta, \theta')$ are translation-invariant in the space of the neurons' preferred stimulus values $(-\pi, \pi)$, allowing the network to hold a continuous family of stationary states (bumps). An external input $I_e(\theta, t)$ containing the stimulus information triggers a bump state (red curve) at the corresponding location in the network.

(B) Model of a synaptic connection with short-term potentiation. In response to a presynaptic spike train (bottom), the neurotransmitter release probability u increases and the fraction of available neurotransmitter x decreases (middle), representing synaptic facilitation and depression. Effective synaptic efficacy is proportional to ux (top).

(C) Firing rate of neurons (top) and sequence of events (bottom; target and mask signal) when simulating conscious working memory with $A_{mask} = 50\text{Hz} < A_{critical}$.

(D) Same as in (C) for non-conscious working memory when $A_{mask} = 65\text{Hz} > A_{critical}$.

(E, F) Performance of the network (distribution of responses) when mask amplitude was near the critical level, $A_{mask} = 62\text{Hz} \sim A_{critical}$, and noise had been added to the system. Out of 4000 trials, 2035 resulted in the conscious (E) and the remainder in the non-conscious regime (F). In both cases, performance remained above chance with the responses concentrated around the initial target location.

Figure 2 – Figure Supplement 1. Perceptual sensitivity does not correlate with working memory performance on unseen trials

(A) Scatter plots depicting the relationship between detection *d*' and accuracy (left), the rate of correct responding (middle), and precision (right) in the working memory task of experiment 1 as a function of visibility.

(B) Same as in (A), but for experiment 2.

Figure 4 – Figure Supplement 1. Alpha- and beta-band desynchronizations serve as a general signature of conscious processing and conscious working memory

(A) Perception task: Topographies represent the power difference (magnetometers) for seen vs target-absent trials (top), seen vs unseen trials (middle), and unseen vs target-absent trials (bottom) in the alpha (8 – 12Hz) and beta (13 – 30Hz) frequency bands as a function of time (0 – 2.1s). Black asterisks indicate sensors showing a significant difference as assessed by a cluster-based permutation test.

(B) Working memory task: Topographies and panels are as in (A).

(C) Working memory task: Topographies represent the power difference (magnetometers) for unseen correct vs target-absent trials (top), unseen incorrect vs target-absent trials (middle), and unseen correct vs unseen incorrect trials (bottom) in the alpha (8 – 12Hz) and beta (13 – 30Hz) frequency bands as a function of time (0 – 2.1s). Black asterisks indicate sensors showing a significant difference as assessed by a cluster-based permutation test.

Figure 4 – Figure Supplement 2. Seen and unseen correct trials do not share the same discriminative decoding axis

(A) Temporal generalization matrices for a decoder trained on the ERFs to distinguish seen from unseen trials in the perception task and tested in the working memory task, either with the same labels (visibility decoder; left) or the unseen correct and incorrect trials (accuracy decoder; right). In each panel, a classifier was trained at every time sample (y-axis) and tested

on all other time points (x-axis). The diagonal gray line demarks classifiers trained and tested on the same time sample. Please note the additional event marker: Mean reaction time (target-present trials) for the visibility response is indicated as a horizontal, dotted line. Any classifier beyond this point only reflects post-visibility processes. Time courses of diagonal decoding are shown as black insets. Thick lines indicate significant, above-chance decoding (Wilcoxon signed-rank test across subjects, uncorrected, one-tailed). For display purposes, data were smoothed using a moving average with a window of eight samples. AUC = area under the curve.

(B) Same as in (A), except that the decoder was trained and tested on average power (relative to baseline) in the alpha band (8 – 12 Hz). For display purposes, data were smoothed using a moving average with a window of one sample.

(C) Same as in (B), except that the decoder was trained and tested on average power (relative to baseline) in the beta band (13 – 30 Hz).

Figure 4 – Figure Supplement 3. Bayesian statistics for the time-frequency analyses

(A) Time courses of average alpha band activity (8 – 12Hz; -0.2 – 2.1s) in a group of frontal sensors as a function of visibility (left) and accuracy on the unseen trials (right; correct = within +/- 2 positions of the actual target location). Shaded area demarks standard error of the mean (SEM) across subjects. Insets show Bayes Factors (as assessed in a two-tailed *t*-test) in four time windows: 0.1 – 0.3s (early), 0.3 – 0.6s (P3b), 0.6 – 1.55s (Del1), and 1.55 – 2.1s (Del2). Del1 = first part of the delay, Del2 = second part of the delay, T = target onset.

(B) Same as in (A), but for average beta band (13 – 30Hz) activity.

Figure 5 – Figure Supplement 1. Representation of seen target locations during conscious perception and working memory

Average time courses of circular-linear correlation coefficients between amplitude of the ERFs and target location on seen trials as a function of task (perception and working memory) in a group of left temporo-occipital (left), occipital (middle), and right temporo-occipital (right) gradiometers. Shaded area demarks standard error of the mean (SEM) across subjects. Mean reaction time (target-present trials) for the visibility response in the perception task is indicated as a vertical, dotted line. Thick line represents significant increase in correlation coefficient as compared to an empirical baseline (one-tailed Wilcoxon signed-rank test across subjects, uncorrected). Insets show average correlation coefficients (relative to baseline) over four time windows: 0.1 – 0.3s (early), 0.3 – 0.6s (P3b), 0.6 – 1.55s (Del1), and 1.55 – 2.5s (Del2). White asterisks denote significant differences to baseline (one-tailed Wilcoxon signed-rank test across subjects), black asterisks significant differences between conditions (two-tailed Wilcoxon signed-rank test across subjects). For display purposes, data were lowpass-filtered at 8Hz. *$p < .05$, **$p < .01$, and ***$p < .001$. Del1 = first part of the delay period, Del2 = second part of the delay period, T = target onset.

Figure 5 – Figure Supplement 2. Circular-linear correlations and multivariate decoding reveal similar time courses for target location

(A) Average time courses of circular-linear correlation coefficients between amplitude of the ERFs and target location as a function of task (perception and working memory) and visibility (seen and unseen) in a group of left temporo-occipital gradiometers. Shaded area demarks standard error of the mean (SEM) across subjects. Thick line represents significant increase in correlation coefficient as compared to an empirical baseline (one-tailed Wilcoxon signed-rank test across subjects, uncorrected). Insets show average correlation coefficients (relative to baseline) over four time windows: 0.1 – 0.3s (early), 0.3 – 0.6s (P3b), 0.6 – 1.55s (Del1), and 1.55 – 2.5s (Del2). White asterisks denote significant differences to baseline (one-tailed

Wilcoxon signed-rank test across subjects). For display purposes, data were lowpass-filtered at 8Hz. *$p < .05$, **$p < .01$, and ***$p < .001$. Del1 = first part of the delay period, Del2 = second part of the delay period, T = target onset.

(B) Average time courses of a linear support vector regression trained to predict target angle as a function of task (perception and working memory) and visibility (seen and unseen). Thick line represents significant increase in decoding accuracy (in radians) as compared to a baseline (one-tailed Wilcoxon signed-rank test across subjects, uncorrected). Insets show average correlation coefficients (relative to baseline) over four time windows: 0.1 – 0.3s (early), 0.3 – 0.6s (P3b), 0.6 – 1.55s (Del1), and 1.55 – 2.5s (Del2). White asterisks denote significant differences to baseline (one-tailed Wilcoxon signed-rank test across subjects). For display purposes, data were lowpass-filtered at 8Hz. *$p < .05$, **$p < .01$, and ***$p < .001$. Del1 = first part of the delay period, Del2 = second part of the delay period, T = target onset.

Figure 5 – Figure Supplement 3. Tracking target/response location on unseen correct and incorrect trials with multivariate decoding

(A) Average time courses of a linear support vector regression trained on seen correct trials to predict target angle on the unseen correct (top) and unseen incorrect (bottom) trials. Thick line represents significant increase in decoding accuracy (in radians) as compared to a baseline (one-tailed Wilcoxon signed-rank test across subjects, uncorrected). Insets show average correlation coefficients (relative to baseline) over four time windows: 0.1 – 0.3s (early), 0.3 – 0.6s (P3b), 0.6 – 1.55s (Del1), and 1.55 – 2.5s (Del2). White asterisks denote significant differences to baseline (one-tailed Wilcoxon signed-rank test across subjects). For display purposes, data were lowpass-filtered at 8Hz. *$p < .05$, **$p < .01$, and ***$p < .001$. Del1 = first part of the delay period, Del2 = second part of the delay period, T = target onset.

(B) Same as in (A), but for response location.

Figure 6 – Figure Supplement 1. Topographies for circular-linear correlations with response location as a function of visibility

Topographies of circular-linear correlations with response location as a function of time for seen (left) and unseen (right) trials. The first three time bins are relative to target, the last two relative to response screen onset. R = response screen onset.

Figure 6 – Figure Supplement 2. Circular-linear correlations and multivariate decoding reveal similar time courses for response location

(A) Average time courses of circular-linear correlation coefficients between amplitude of the ERFs and response location as a function of task (perception and working memory) and visibility (seen and unseen) in a group of left temporo-occipital gradiometers. Shaded area demarks standard error of the mean (SEM) across subjects. Thick line represents significant increase in correlation coefficient as compared to an empirical baseline (one-tailed Wilcoxon signed-rank test across subjects, uncorrected). Insets show average correlation coefficients (relative to baseline) over four time windows: 0.1 – 0.3s (early), 0.3 – 0.6s (P3b), 0.6 – 1.55s (Del1), and 1.55 – 2.5s (Del2). White asterisks denote significant differences to baseline (one-tailed Wilcoxon signed-rank test across subjects). For display purposes, data were lowpass-filtered at 8Hz. *$p < .05$, **$p < .01$, and ***$p < .001$. Del1 = first part of the delay period, Del2 = second part of the delay period, T = target onset.

(B) Average time courses of a linear support vector regression trained to predict response angle as a function of task (perception and working memory) and visibility (seen and unseen). Thick line represents significant increase in decoding accuracy (in radians) as compared to a baseline (one-tailed Wilcoxon signed-rank test across subjects, uncorrected). Insets show average correlation coefficients (relative to baseline) over four time windows: 0.1 – 0.3s

(early), 0.3 – 0.6s (P3b), 0.6 – 1.55s (Del1), and 1.55 – 2.5s (Del2). White asterisks denote significant differences to baseline (one-tailed Wilcoxon signed-rank test across subjects). For display purposes, data were lowpass-filtered at 8Hz. *$p < .05$, **$p < .01$, and ***$p < .001$. Del1 = first part of the delay period, Del2 = second part of the delay period, T = target onset.

Tables

Training → Testing		0.1 – 0.3s		0.3 – 0.6s		0.6 – 1.55s		1.55 – 2.5s	
		AUC (SEM)	*p*	AUC (SEM)	*p*	AUC (SEM)	*p*	AUC (SEM)	*p*
P → P	Diagonal	0.53 (0.01)	**.004**[a]	0.58 (0.01)	**.001**[a]	0.56 (0.01)	**.001**[a]	0.52 (0.01)	.058[a]
	P3b	0.51 (0.01)	.152[b]	0.55 (0.01)	**.003**[b]	0.52 (0.01)	.064[b]	0.51 (0.005)	.101[b]
	Maintenance	0.50 (0.004)	.507[b]	0.50 (0.005)	.382[b]	0.52 (0.01)	**.046**[b]	0.51 (0.01)	.382[b]
P → WM	Diagonal	0.52 (0.005)	**.003**[a]	0.55 (0.01)	**.001**[a]	0.53 (0.005)	**.001**[a]	0.50 (0.01)	.486[a]
	P3b	0.50 (0.004)	.279[b]	0.53 (0.01)	**.011**[b]	0.51 (0.01)	.101[b]	0.49 (0.01)	.101[b]
	Maintenance	0.49 (0.005)	**.039**[b]	0.49 (0.01)	.311[b]	0.51 (0.006)	.279[b]	0.50 (0.01)	.972[b]
WM → WM	Diagonal	0.52 (0.01)	.066[a]	0.57 (0.02)	**.007**[a]	0.55 (0.01)	**.001**[a]	0.52 (0.01)	.173[a]
	P3b	0.50 (0.01)	.807[b]	0.54 (0.01)	**.020**[b]	0.50 (0.01)	.807[b]	0.49 (0.01)	.422[b]
	Maintenance	0.50 (0.01)	.507[b]	0.49 (0.01)	.552[b]	0.51 (0.01)	.650[b]	0.51 (0.01)	.600[b]
WM → P	Diagonal	0.52 (0.005)	**.010**[a]	0.55 (0.01)	**.001**[a]	0.53 (0.01)	**.014**[a]	0.51 (0.01)	.276[a]
	P3b	0.50 (0.006)	.753[b]	0.53 (0.01)	**.016**[b]	0.50 (0.01)	.972[b]	0.49 (0.01)	.463[b]
	Maintenance	0.49 (0.01)	.279[b]	0.49 (0.01)	.101[b]	0.51 (0.01)	.701[b]	0.50 (0.01)	.972[b]

Table 1. Statistics for decoding analyses

Statistics are shown for decoding of visibility category (seen vs. unseen) as a function of task and testing time bin. The first column identifies the respective training and testing sets (P = perception task; WM = working memory task), the second column the training classifiers (Diagonal = diagonal, P3b = 300 – 600ms, Maintenance = 0.8 – 2.5s), that were averaged. Bold numbers indicate above-chance decoding performance ([a]one-tailed, [b]two-tailed Wilcoxon signed-rank test across subjects). AUC = area under the curve; SEM = standard error of the mean (across participants).

		0.1 – 0.3s: Target		0.3 – 0.6s: Target		0.6 – 1.55s: Target		1.55 – 2.5s: Target		-0.5 – 0s: Resp		0 – 0.8s: Resp	
		Δ*rho* (SEM)	*p*	Δ*rho* (SEM)	*p*	Δ*rho* (SEM)	*p*	Δ*rho* (SEM)	*p*	Δ*rho* (SEM)	*p*	Δ*rho* (SEM)	*p*
Distractor													
All	Occ	0.021 (0.005)	< **.001**	0.015 (0.005)	**.009**	n/a		n/a		n/a		n/a	
Target													
All	Occ	0.021 (0.005)	< **.001**	0.030 (0.007)	< **.001**	0.004 (0.002)	.064	0.002 (0.020)	.108	n/a		n/a	
P Seen	L Temp	0.011 (0.004)	**.007**	0.014 (0.005)	**.009**	0.005 (0.002)	**.029**	-0.002 (0.002)	.830	n/a		n/a	
	Occ	0.004 (0.004)	.207	0.019 (0.003)	< **.001**	0.003 (0.003)	.153	-0.001 (0.002)	.751	n/a		n/a	
	R Temp	0.012 (0.004)	**.011**	0.030 (0.004)	< **.001**	0.008 (0.002)	**.001**	-0.003 (0.002)	.905	n/a		n/a	
Seen	L Temp	0.018 (0.005)	< **.001**	0.021 (0.004)	< **.001**	0.006 (0.003)	**.024**	-0.002 (0.002)	.729	n/a		n/a	
	Occ	0.024 (0.006)	**.001**	0.031 (0.008)	< **.001**	0.009 (0.004)	**.024**	0.001 (0.003)	.446	n/a		n/a	
	R Temp	0.016 (0.008)	.064	0.031 (0.006)	< **.001**	0.005 (0.004)	.064	0.001 (0.003)	.342	n/a		n/a	
Unseen	L Temp	0.009 (0.004)	**.047**	0.007 (0.004)	.084	-0.004 (0.002)	.971	$-2.9*10^{-4}$ (0.002)	.527	n/a		n/a	
	Occ	0.011 (0.005)	**.024**	0.007 (0.004)	.055	-0.006 (0.003)	.966	$3.0*10^{-4}$ (0.003)	.446	n/a		n/a	
	R Temp	-0.002 (0.005)	.632	0.002 (0.002)	.527	-0.003 (0.002)	.936	0.002 (0.004)	.473	n/a		n/a	
Unseen+	L Temp	0.014 (0.006)	**.040**	-0.002 (0.007)	.682	0.002 (0.004)	.271	-0.002 (0.005)	.812	n/a		n/a	
	Occ	0.007 (0.007)	.227	0.007 (0.007)	.170	-0.001 (0.006)	.554	$2.2*10^{-4}$ (0.005)	.580	n/a		n/a	
	R Temp	-0.012 (0.008)	.803	-0.010 (0.007)	.905	-0.004 (0.005)	.706	-0.005 (0.006)	.812	n/a		n/a	
Unseen-	L Temp	0.006 (0.009)	.500	0.002 (0.010)	.554	-0.006 (0.004)	.916	0.001 (0.005)	.393	n/a		n/a	
	Occ	0.001 (0.005)	.580	-0.012 (0.006)	.966	-0.009 (0.004)	.980	-0.007 (0.003)	.989	n/a		n/a	
	R Temp	-0.012 (0.007)	.971	-0.003 (0.004)	.847	-0.006 (0.005)	.916	$-8.6*10^{-5}$(0.004)	.420	n/a		n/a	
Response													
Seen	L Temp	0.015 (0.005)	**.002**	0.020 (0.005)	**.005**	0.005 (0.002)	**.020**	$-1.2*10^{-4}$ (0.002)	.420	-0.001 (0.003)	.527	0.022 (0.005)	**.001**
	Occ	0.018 (0.007)	**.020**	0.029 (0.007)	< **.001**	0.008 (0.003)	**.007**	0.003 (0.004)	.207	$4.3*10^{-4}$(0.003)	.446	0.020 (0.004)	< **.001**
	R Temp	0.014 (0.009)	.122	0.030 (0.006)	< **.001**	0.005 (0.004)	.137	$6.2*10^{-4}$(0.003)	.473	$4.9*10^{-4}$ (0.005)	.318	0.025 (0.004)	< **.001**
	Frontal	0.006 (0.005)	.170	0.006 (0.004)	.122	0.006 (0.003)	**.034**	0.003 (0.003)	.073	0.004 (0.005)	.249	0.034 (0.007)	< **.001**
Unseen	L Temp	0.006 (0.004)	.084	-0.001 (0.004)	.500	0.003 (0.002)	.064	0.005 (0.003)	.137	0.004 (0.006)	.294	0.012 (0.003)	< **.001**
	Occ	0.003 (0.005)	.294	$-5.1*10^{-4}$ (0.003)	.394	0.003 (0.002)	.108	0.006 (0.004)	.096	0.009 (0.006)	.170	0.017 (0.004)	< **.001**
	R Temp	-0.003 (0.005)	.773	-0.002 (0.006)	.368	$-9.9*10^{-4}$ (0.003)	.446	$9.7*10^{-4}$ (0.003)	.393	0.002 (0.006)	.473	0.015 (0.005)	**.004**
	Frontal	0.001 (0.004)	.473	0.009 (0.003)	**.006**	0.002 (0.003)	.137	0.007 (0.002)	**.003**	$6.4*10^{-4}$(0.004)	.682	0.027 (0.007)	**.002**
Unseen+	L Temp	0.008 (0.007)	.096	0.002 (0.007)	.446	0.005 (0.003)	.108	0.002 (0.005)	.446	0.014 (0.007)	.055	0.012 (0.007)	**.024**
	Occ	-0.003 (0.009)	.580	0.004 (0.008)	.393	0.002 (0.005)	.393	0.002 (0.005)	.473	0.014 (0.007)	.170	0.006 (0.006)	.227
	R Temp	-0.012 (0.008)	.878	-0.005 (0.006)	.773	-0.004 (0.005)	.729	-0.005 (0.005)	.830	0.008 (0.007)	.170	0.014 (0.008)	.084
	Frontal	0.001 (0.008)	.318	0.006 (0.006)	.122	-0.004 (0.004)	.892	0.005 (0.004)	.342	0.005 (0.006)	.227	0.024 (0.007)	**.004**
Unseen-	L Temp	0.008 (0.005)	.096	$8.3*10^{-4}$ (0.005)	.446	0.004 (0.003)	.153	0.003 (0.004)	.207	-0.003 (0.006)	.632	0.011 (0.004)	**.024**
	Occ	0.013 (0.009)	.122	0.009 (0.007)	.096	0.003 (0.003)	.153	0.003 (0.006)	.342	0.003 (0.005)	.227	0.014 (0.006)	**.020**
	R Temp	-0.005 (0.008)	.812	-0.009 (0.005)	.916	-0.004 (0.004)	.905	-0.002 (0.005)	.682	0.002 (0.005)	.368	0.007 (0.006)	.137
	Frontal	-0.007 (0.006)	.863	-0.003 (0.004)	.729	0.004 (0.004)	.207	-0.010 (0.003)	.527	-0.005 (0.003)	.927	0.018 (.007)	**.011**

Table 2. Statistics for circular-linear correlation analyses

Statistics for circular-linear correlation analyses between the average amplitude of the MEG signal in the gradiometers and distractor, target, and response position are listed as a function of visibility, accuracy, channel group and time window. The first four time windows are relative to target onset, the last two relative to the onset of the response screen. Bold numbers indicate significant differences in correlation values relative to an empirical baseline (one-tailed Wilcoxon signed-rank test). Frontal = frontal gradiometers; L Temp = left temporo-occipital gradiometers; Occ = occipital gradiometers; P = perception task; Resp = response; R Temp = right temporo-occipital gradiometers; SEM = standard error of the mean (across subjects); Unseen+ = unseen correct trials (within +/- 2 positions of actual target location); Unseen- = unseen incorrect trials.

BF		0.1 – 0.3s: Target	0.3 – 0.6s: Target	0.6 – 1.55s: Target	1.55 – 2.5s: Target	-0.5 – 0: Resp	0 – 0.8: Resp
Distractor							
All	Occ	**46.72**	**14.47**	n/a	n/a	n/a	n/a
Target							
All	Occ	**109.60**	**125.33**	2.29	0.77	n/a	n/a
P Seen	L Temp	**4.84**	**10.03**	**3.62**	0.16	n/a	n/a
	Occ	0.68	**496.64**	0.96	0.21	n/a	n/a
	R Temp	**6.81**	**5256.15**	**23.35**	0.13	n/a	n/a
Seen	L Temp	**24.07**	**175.81**	**3.89**	0.17	n/a	n/a
	Occ	**56.90**	**45.43**	**3.77**	0.40	n/a	n/a
	R Temp	2.31	**496.24**	1.22	0.38	n/a	n/a
Unseen	L Temp	2.58	1.33	0.11	0.28	n/a	n/a
	Occ	**3.34**	1.53	0.11	0.30	n/a	n/a
	R Temp	0.23	0.48	0.14	0.47	n/a	n/a
Unseen+	L Temp	**3.75**	0.22	0.46	0.21	n/a	n/a
	Occ	0.76	0.65	0.24	0.29	n/a	n/a
	R Temp	0.13	0.13	0.18	0.16	n/a	n/a
Unseen-	L Temp	0.49	0.32	0.13	0.34	n/a	n/a
	Occ	0.35	0.11	0.11	0.11	n/a	n/a
	R Temp	0.12	0.19	0.14	0.28	n/a	n/a
Response							
Seen	L Temp	**11.35**	**41.95**	**4.16**	0.27	0.23	**90.13**
	Occ	**7.41**	**56.46**	**4.60**	0.56	0.31	**152.61**
	R Temp	1.42	**330.43**	0.95	0.32	0.30	**606.35**
	Frontal	1.05	1.12	2.42	0.57	0.60	**127.23**
Unseen	L Temp	1.28	0.23	1.37	1.05	0.52	**137.36**
	Occ	0.44	0.25	0.98	1.32	1.24	**49.11**
	R Temp	0.18	0.22	0.23	0.35	0.35	**13.73**
	Frontal	0.35	**12.69**	0.47	**15.86**	0.32	**41.58**
Unseen+	L Temp	0.85	0.33	2.19	0.38	2.25	2.05
	Occ	0.23	0.43	0.38	0.35	2.10	0.66
	R Temp	0.13	0.17	0.18	0.17	0.78	1.90
	Frontal	0.32	0.82	0.14	0.77	0.59	**16.76**
Unseen-	L Temp	1.47	0.32	1.15	0.50	0.20	**5.13**
	Occ	1.23	0.94	0.84	0.44	0.47	**3.45**
	R Temp	0.19	0.12	0.16	0.21	0.36	0.88
	Frontal	0.15	0.18	0.69	0.23	0.13	**5.14**

Table 3. Bayes Factors for circular-linear correlation analyses

Bayes Factors for circular-linear correlation analyses between the average amplitude of the MEG signal in the gradiometers and distractor, target, and response position are shown as a function of visibility, accuracy, channel group and time window. The first four time windows are relative to target onset, the last two relative to the onset of the response screen. Bold numbers indicate strong evidence in favor of the alternative hypothesis (i.e., an increase in correlation values relative to an empirical baseline as assessed by a one-tailed Bayesian *t*-test). Frontal = frontal gradiometers; L Temp = left temporo-occipital gradiometers; Occ = occipital gradiometers; P = perception task; Resp = response; R Temp = right temporo-occipital gradiometers; SEM = standard error of the mean (across subjects); Unseen+ = unseen correct trials (within +/- 2 positions of actual target location); Unseen- = unseen incorrect trials.

Task	Target	Visibility 4 (clearly seen) *M (SD)*	Visibility 3 (weakly seen) *M (SD)*	Visibility 2 (glimpse) *M (SD)*	Visibility 1 (unseen) *M (SD)*
Perception	Present	9.8 (16.6)	17.3 (12.8)	46 (17.8)	61.2 (15.4)
	Absent	0.1 (0.3)	0.5 (1.4)	3.0 (3.8)	28.9 (5.7)
Working memory	Present	10.1 (18.0)	15.8 (14.6)	45.2 (17.8)	57.4 (17.4)
	Absent	0.0 (0.0)	0.2 (0.6)	1.9 (1.9)	29.3 (4.4)

Table 4. Trial counts

Number of trials included in the MEG analyses are listed as a function of task (perception vs. working memory task), target (present vs. absent), and visibility rating. Mean (*M*) and standard deviation (*SD*) are based on 13 participants and all trials retained after preprocessing of the MEG data.

Figure 1

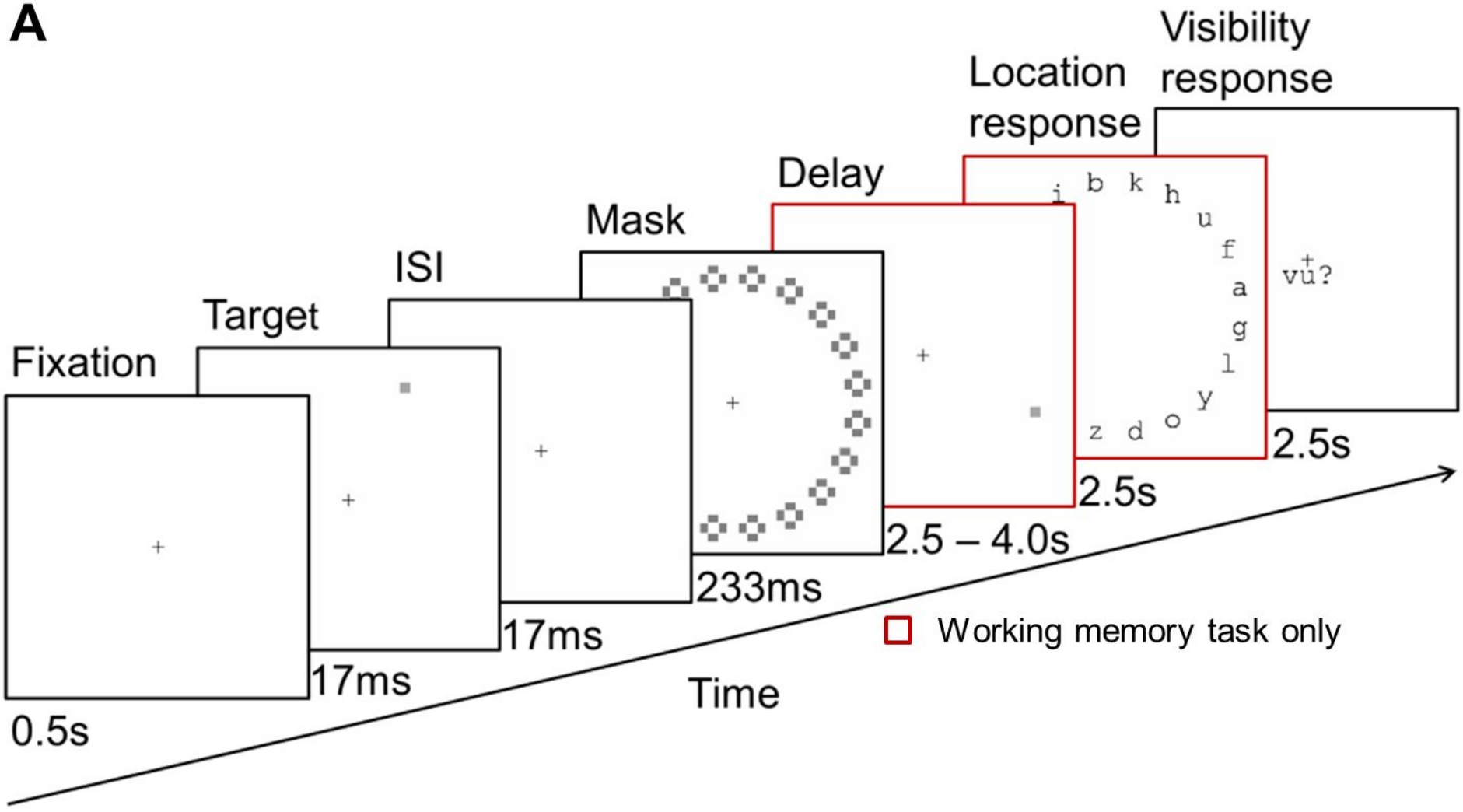
A
Visibility response
Location response
Delay
Mask
ISI
Target
Fixation
0.5s
17ms
17ms
233ms
2.5 – 4.0s
2.5s
2.5s
Working memory task only
Time

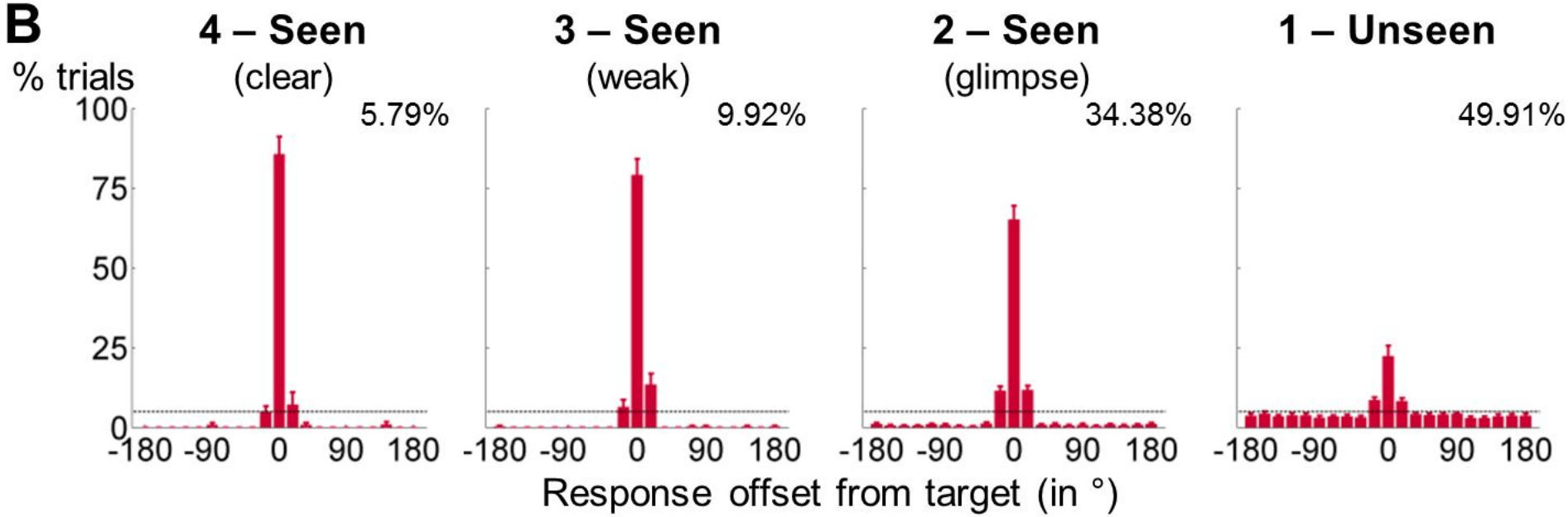
B
4 – Seen (clear)
3 – Seen (weak)
2 – Seen (glimpse)
1 – Unseen
% trials
100
75
50
25
0
5.79%
9.92%
34.38%
49.91%
-180 -90 0 90 180
Response offset from target (in °)

Figure 2

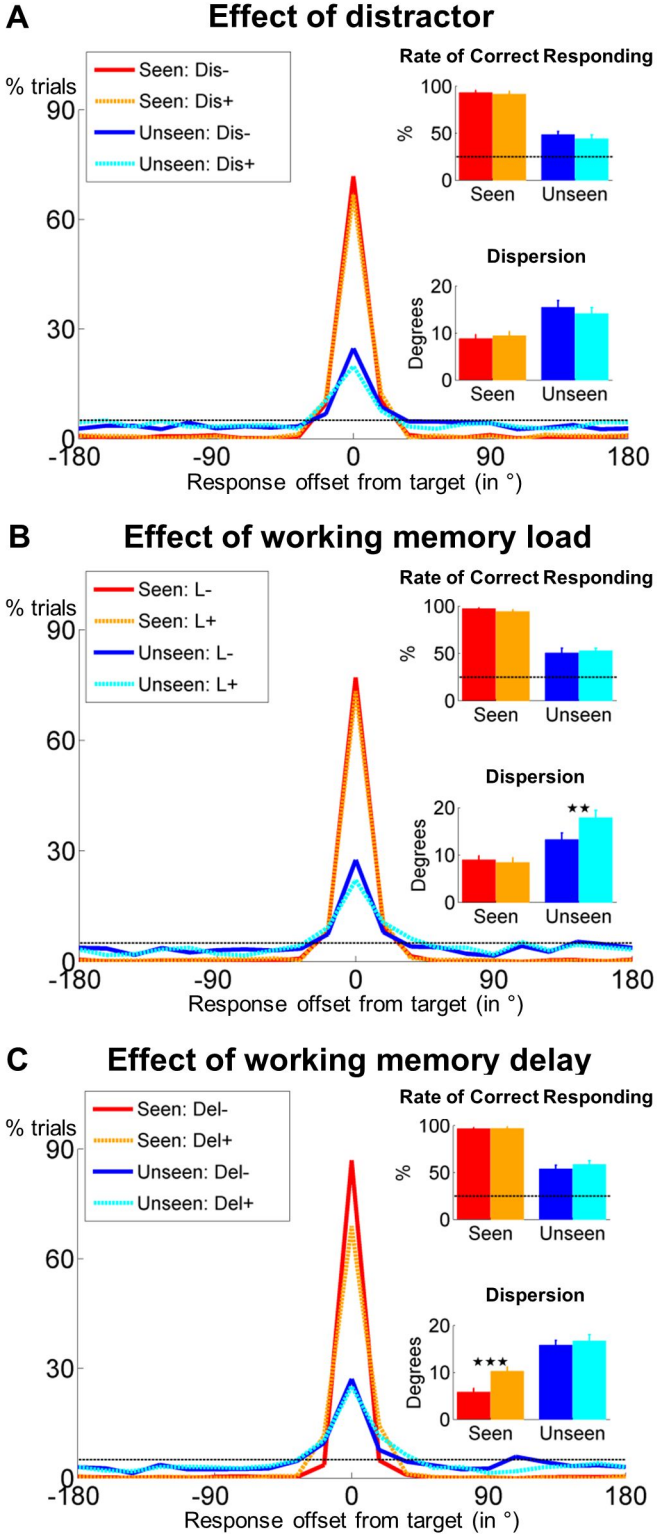
A
Effect of distractor
Seen: Dis-
Seen: Dis+
Unseen: Dis-
Unseen: Dis+
% trials
Rate of Correct Responding
Dispersion
Seen
Unseen
Degrees
Response offset from target (in °)
B
Effect of working memory load
Seen: L-
Seen: L+
Unseen: L-
Unseen: L+
C
Effect of working memory delay
Seen: Del-
Seen: Del+
Unseen: Del-
Unseen: Del+

Figure 3

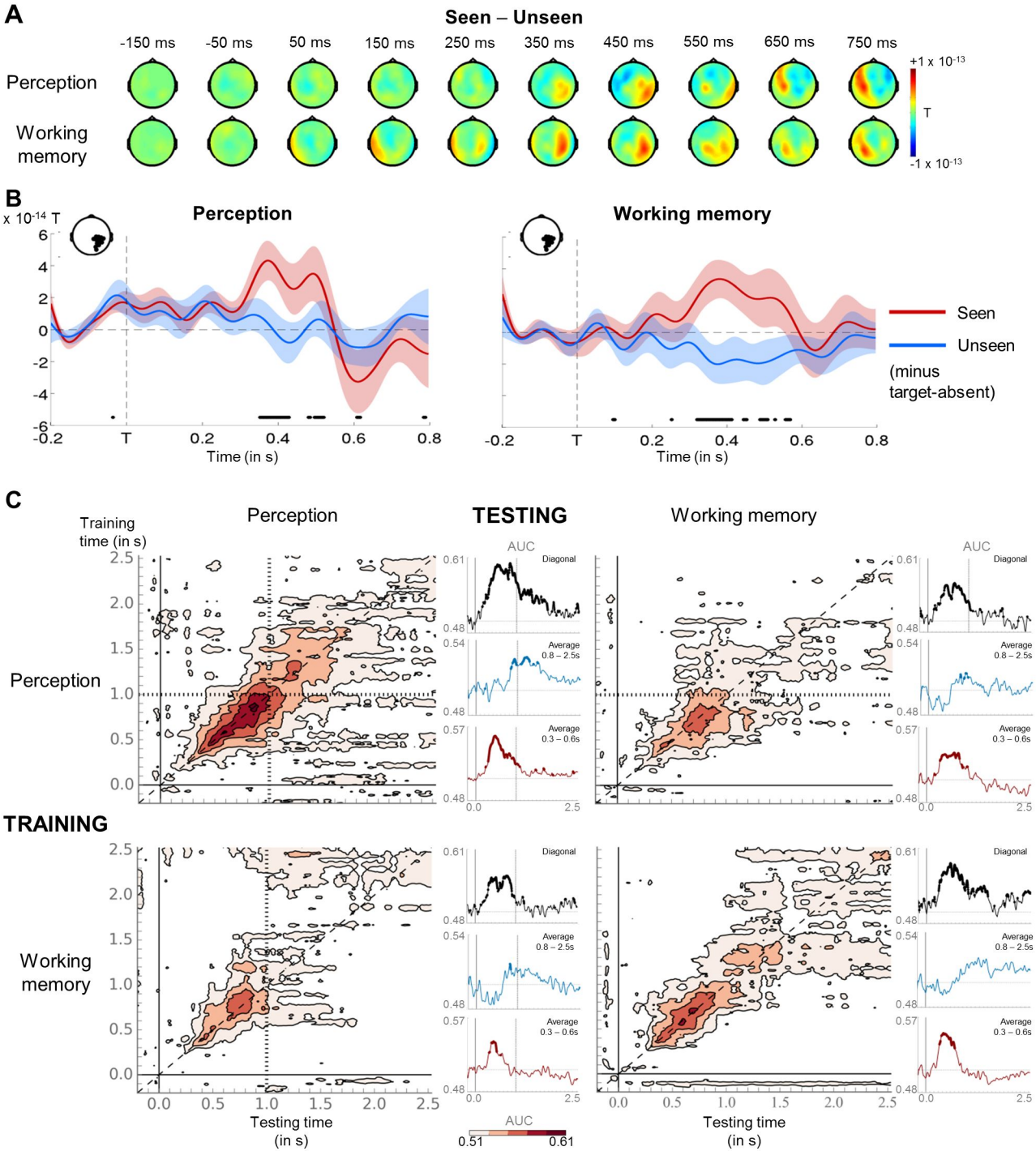
A
Seen – Unseen
-150 ms
-50 ms
50 ms
150 ms
250 ms
350 ms
450 ms
550 ms
650 ms
750 ms
Perception
Working memory
+1 x 10-13
T
-1 x 10-13
B
x 10-14 T
Perception
Working memory
Seen
Unseen
(minus target-absent)
Time (in s)
C
Training time (in s)
Perception
TESTING
Working memory
AUC
Diagonal
Average 0.8 – 2.5s
Average 0.3 – 0.6s
TRAINING
Working memory
Testing time (in s)
AUC

Figure 4

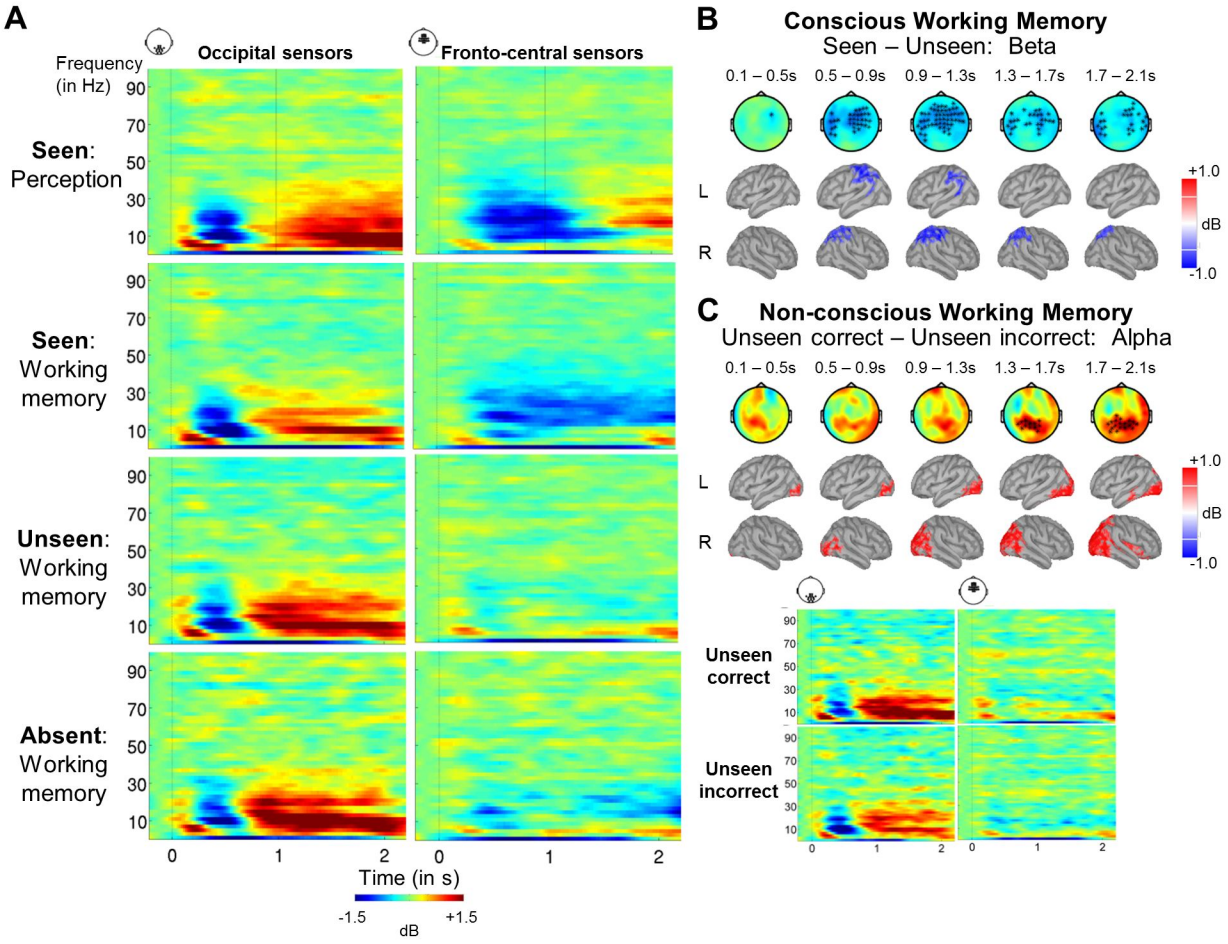
A
Occipital sensors
Fronto-central sensors
Frequency (in Hz)
90
70
50
30
10
Seen: Perception
Seen: Working memory
Unseen: Working memory
Absent: Working memory
0
1
2
Time (in s)
-1.5
+1.5
dB
B
Conscious Working Memory
Seen – Unseen: Beta
0.1 – 0.5s
0.5 – 0.9s
0.9 – 1.3s
1.3 – 1.7s
1.7 – 2.1s
L
R
+1.0
dB
-1.0
C
Non-conscious Working Memory
Unseen correct – Unseen incorrect: Alpha
0.1 – 0.5s
0.5 – 0.9s
0.9 – 1.3s
1.3 – 1.7s
1.7 – 2.1s
L
R
+1.0
dB
-1.0
Unseen correct
Unseen incorrect

Figure 5

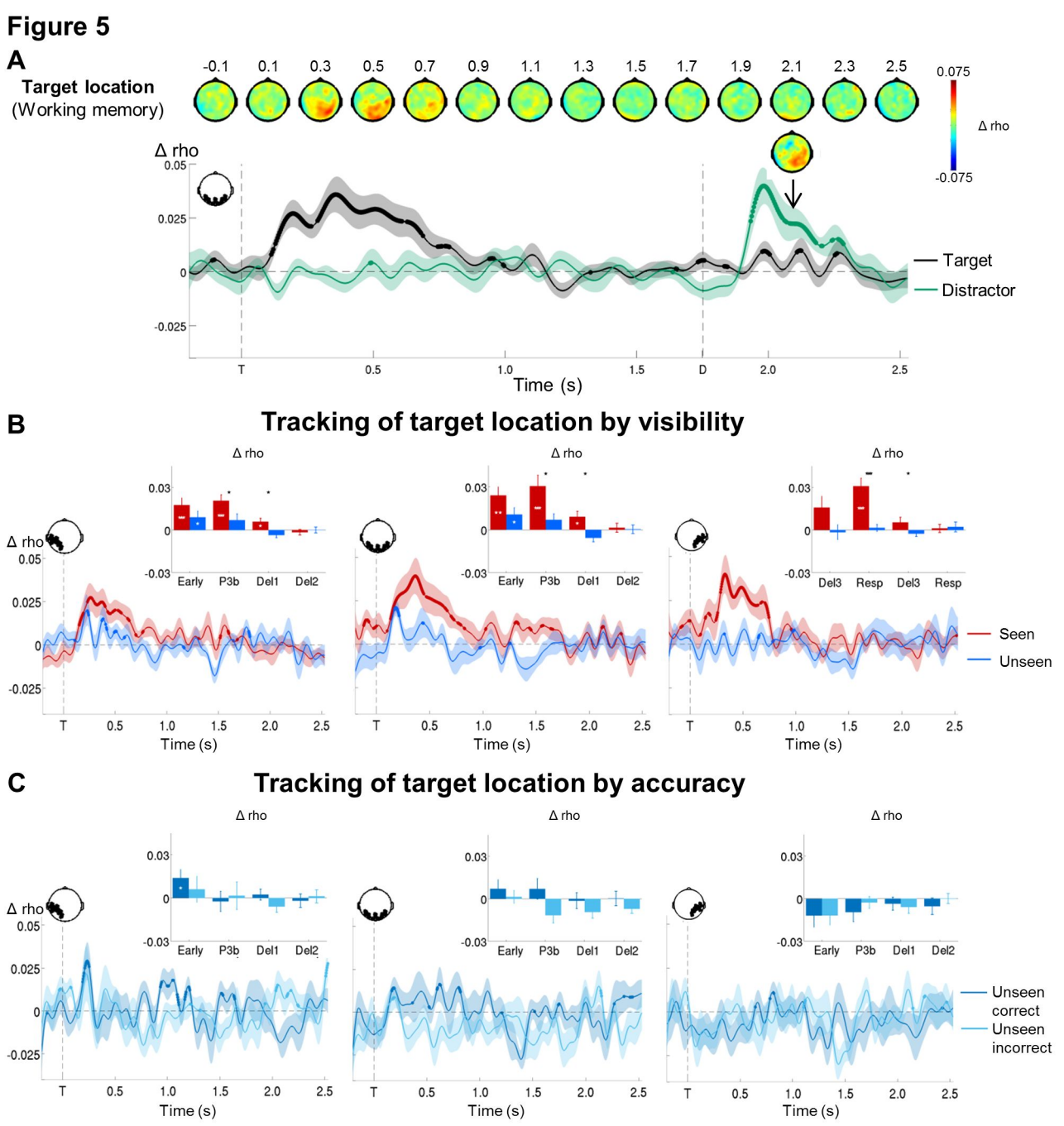
A
Target location
(Working memory)
-0.1
0.1
0.3
0.5
0.7
0.9
1.1
1.3
1.5
1.7
1.9
2.1
2.3
2.5
0.075
Δ rho
-0.075
Δ rho
0.05
0.025
0
-0.025
T
0.5
1.0
1.5
D
2.0
2.5
Time (s)
Target
Distractor
B
Tracking of target location by visibility
Δ rho
0.03
0
-0.03
Early
P3b
Del1
Del2
Del3
Resp
Seen
Unseen
C
Tracking of target location by accuracy
Unseen correct
Unseen incorrect

Figure 6

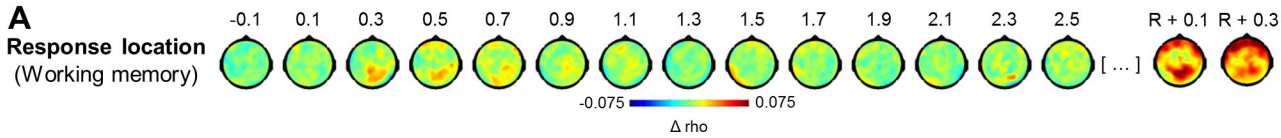
A
Response location
(Working memory)
-0.1
0.1
0.3
0.5
0.7
0.9
1.1
1.3
1.5
1.7
1.9
2.1
2.3
2.5
[…]
R + 0.1
R + 0.3
-0.075
0.075
Δ rho

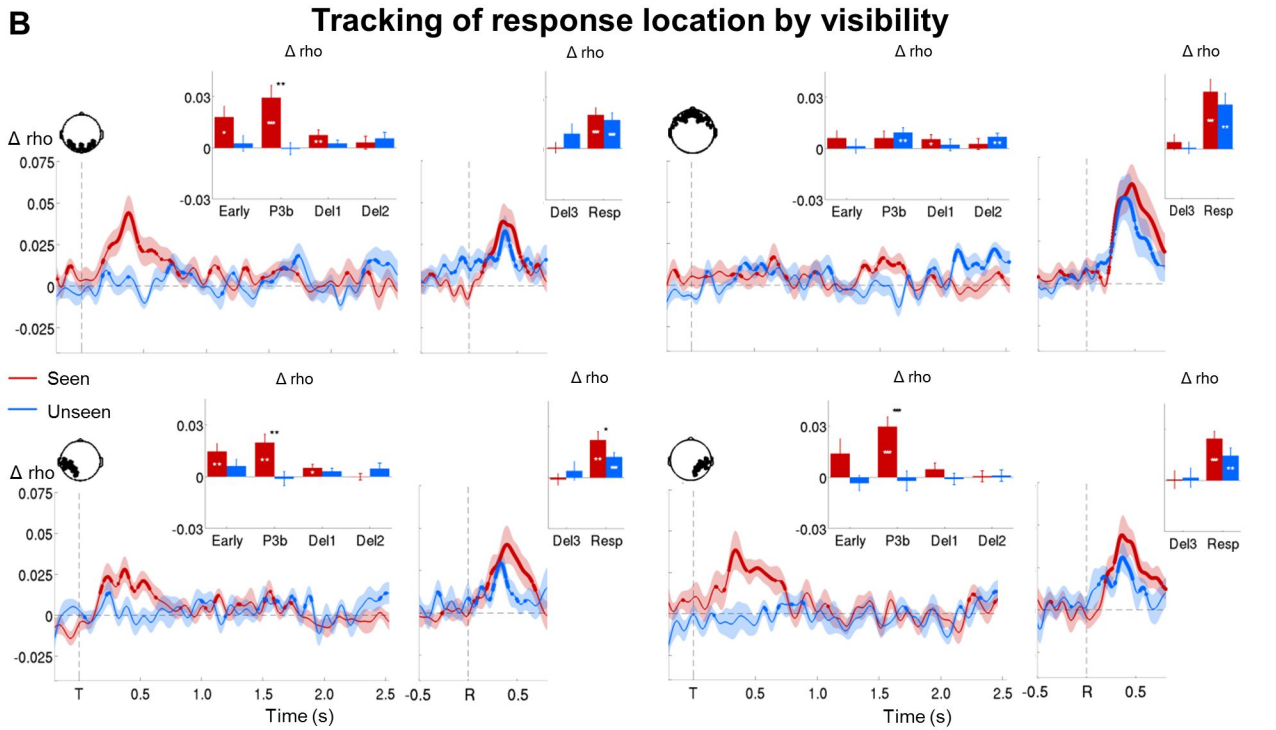
B
Tracking of response location by visibility
Δ rho
Early
P3b
Del1
Del2
Del3
Resp
Seen
Unseen
T
R
Time (s)

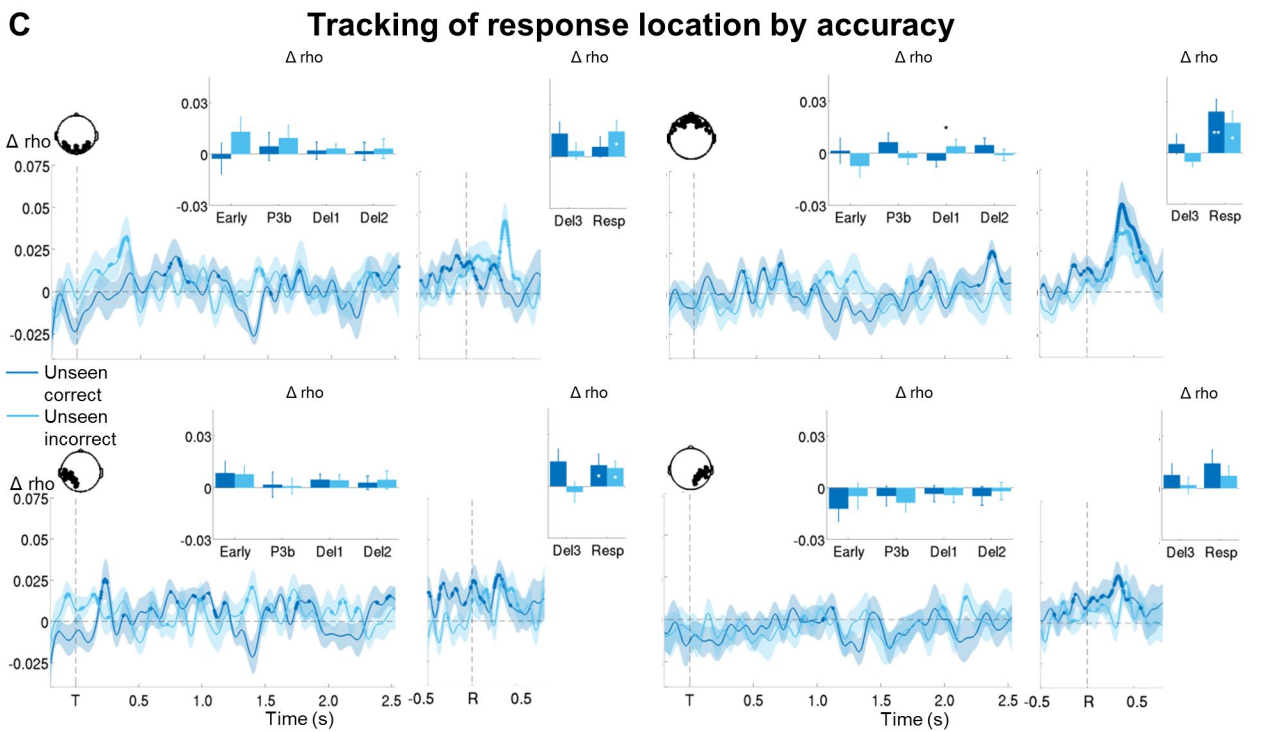
C
Tracking of response location by accuracy
Δ rho
Early
P3b
Del1
Del2
Del3
Resp
Unseen correct
Unseen incorrect
T
R
Time (s)

Figure 7

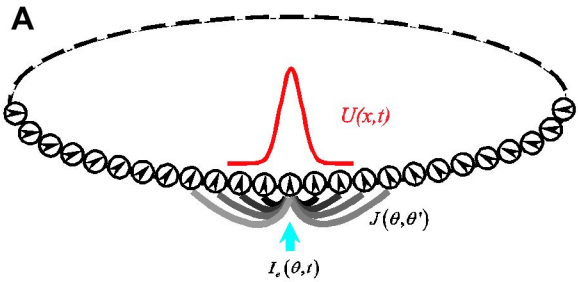
A
U(x,t)
J(θ,θ')
I_e(θ,t)

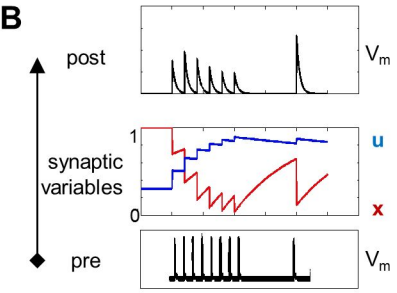
B
post
V_m
synaptic variables
1
0
u
x
pre
V_m

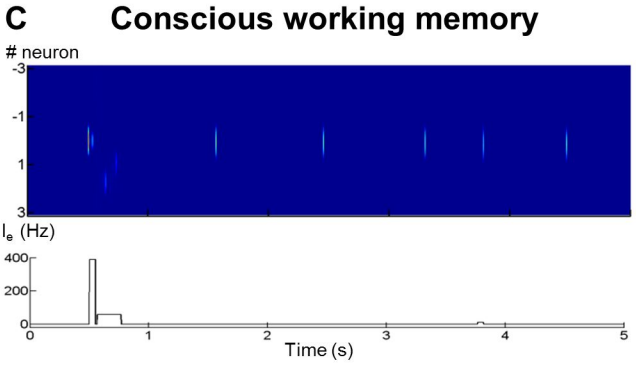
C
Conscious working memory
neuron
-3
-1
1
3
I_e (Hz)
400
200
0
0
1
2
3
4
5
Time (s)

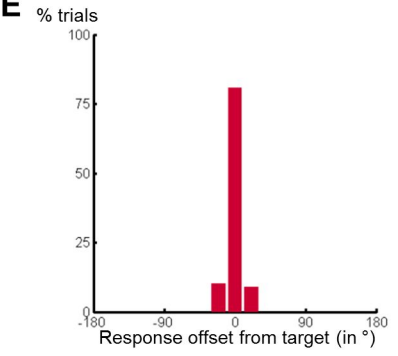
E
% trials
100
75
50
25
0
-180
-90
0
90
180
Response offset from target (in °)

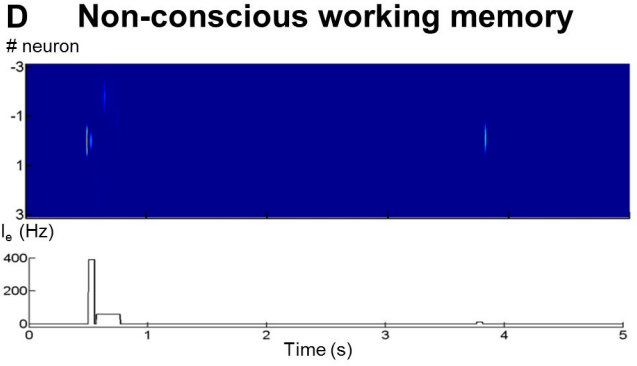
D
Non-conscious working memory
neuron
-3
-1
1
3
I_e (Hz)
400
200
0
0
1
2
3
4
5
Time (s)

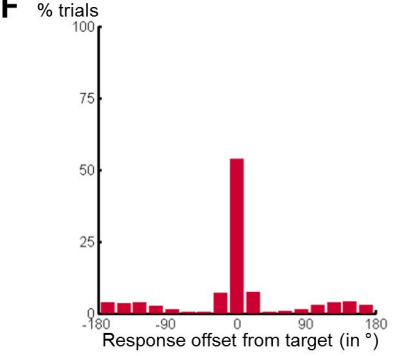
F
% trials
100
75
50
25
0
-180
-90
0
90
180
Response offset from target (in °)

Figure 2 – Figure Supplement 1

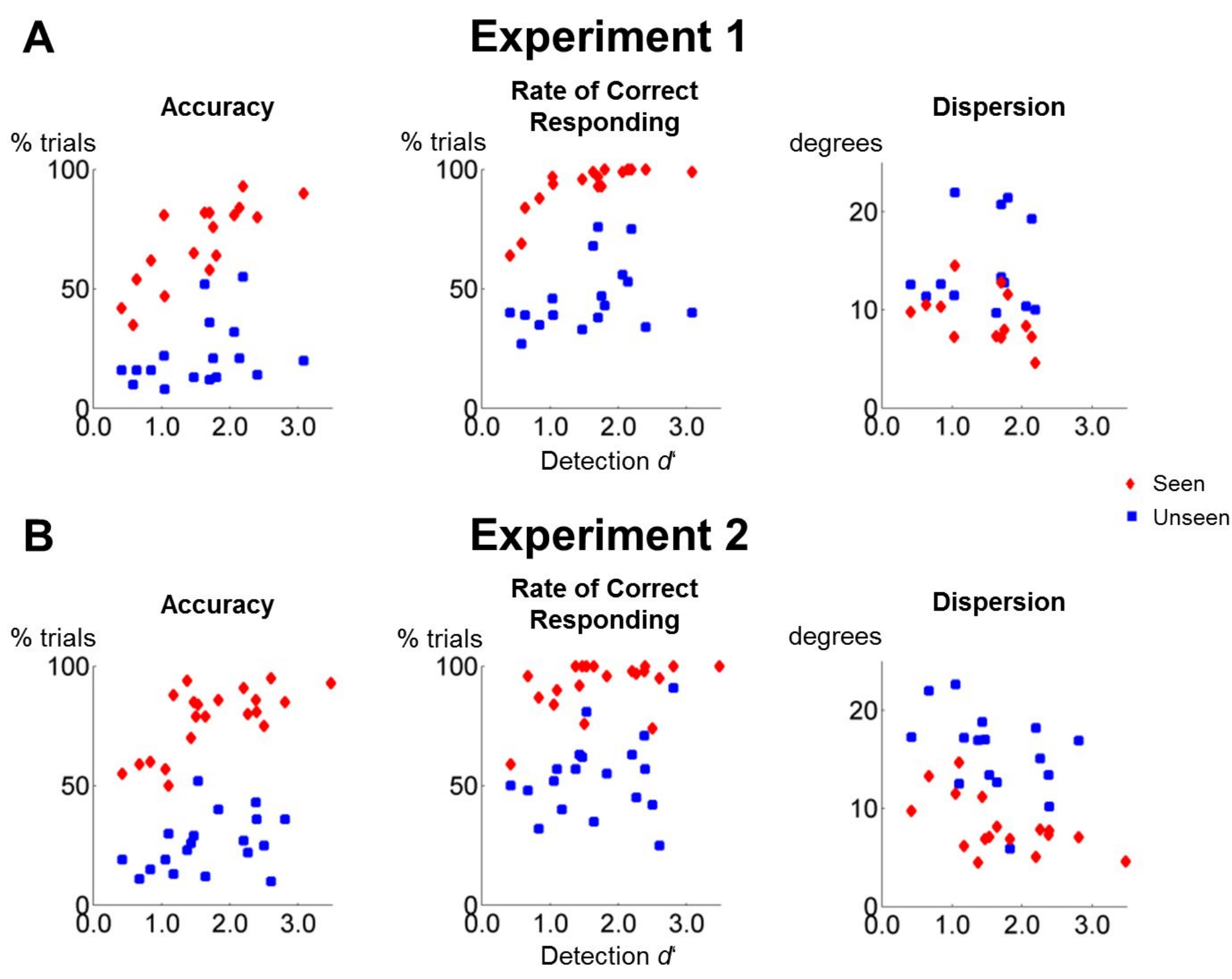

Figure 4 – Figure Supplement 1

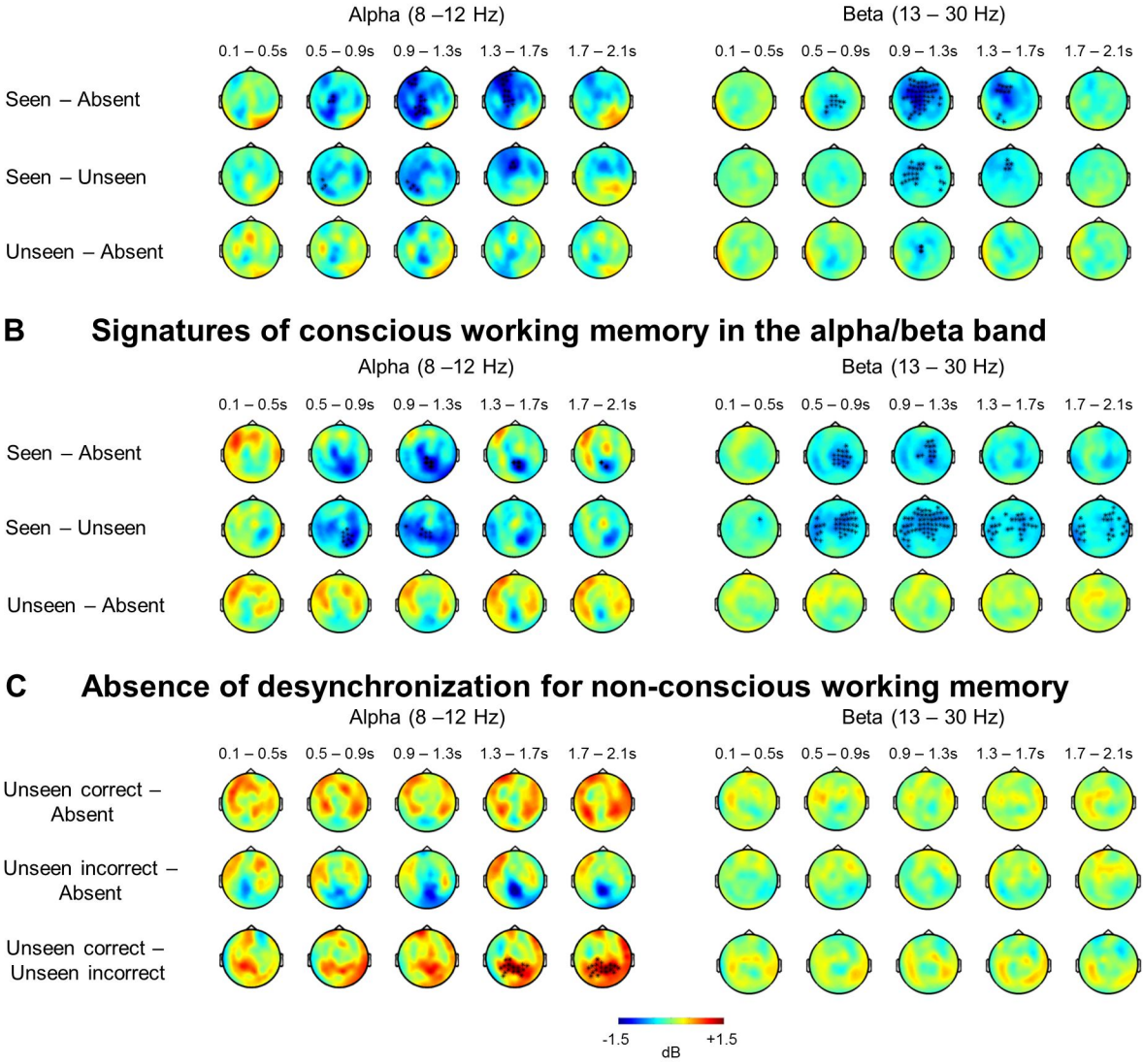

Figure 4 – Figure Supplement 2

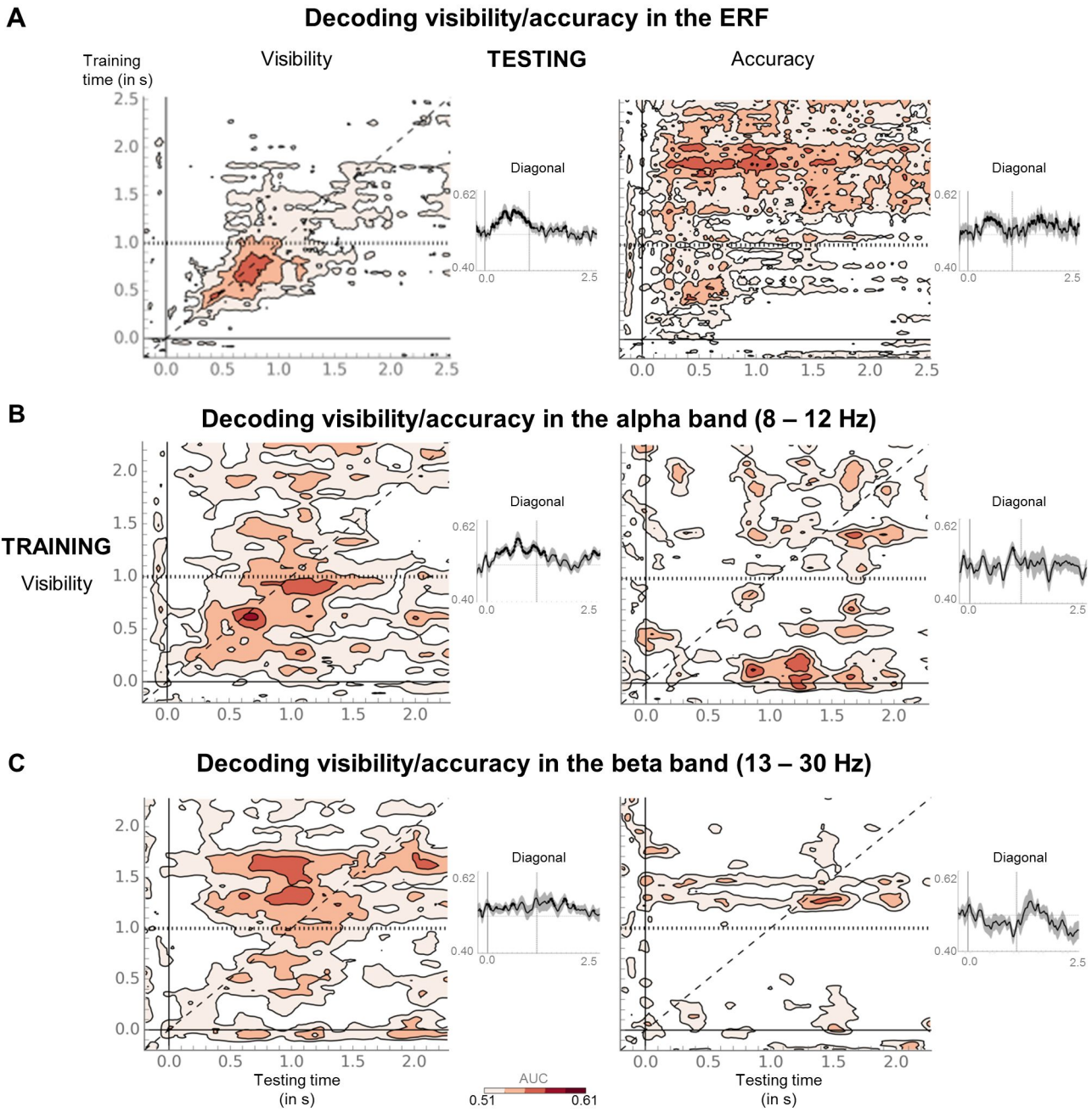

Figure 4 – Figure Supplement 3

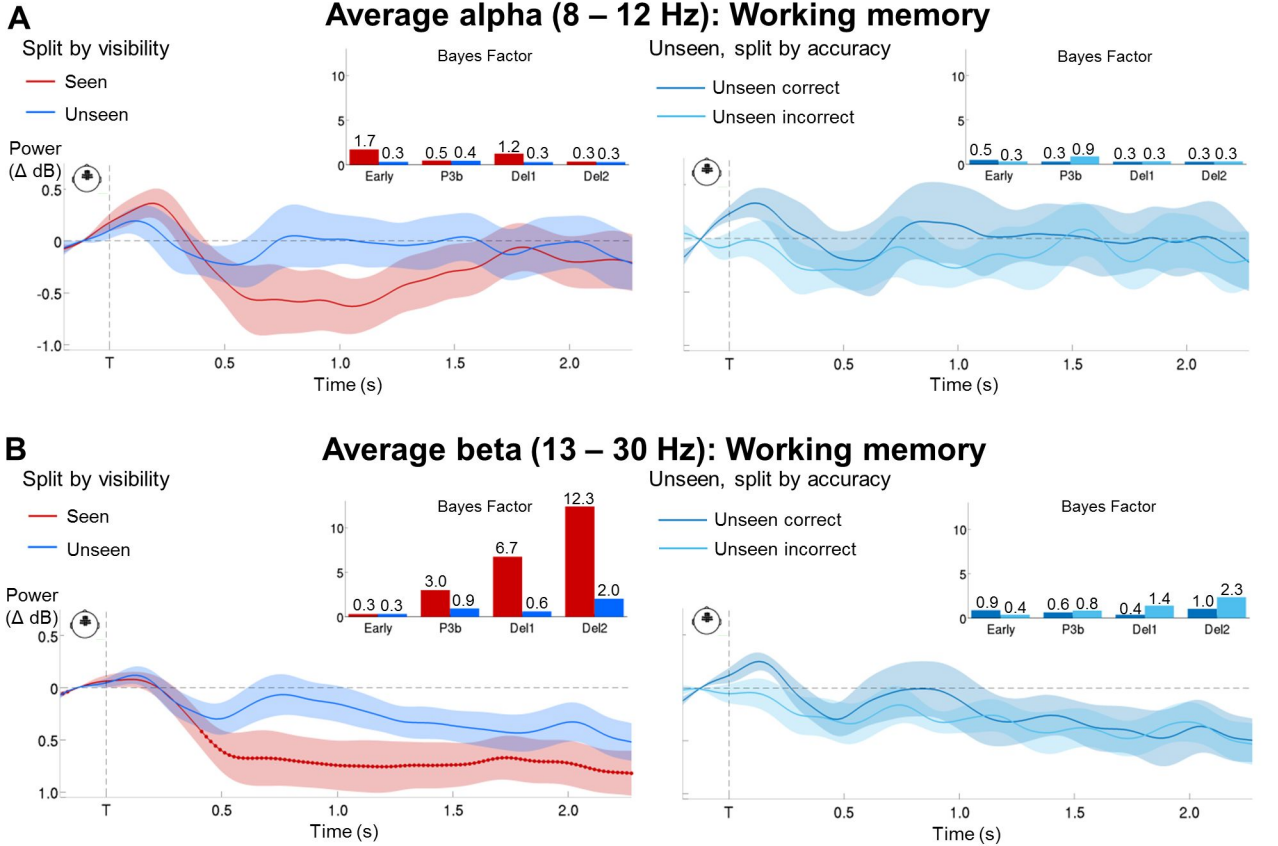

Figure 5 – Figure Supplement 1

Encoding of seen target locations in both tasks

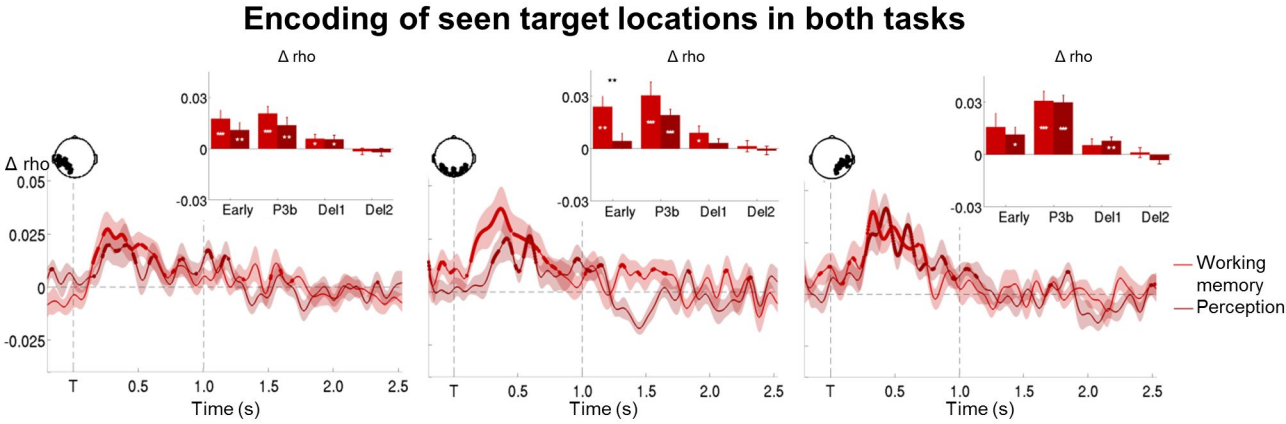

Figure 5 – Figure Supplement 2

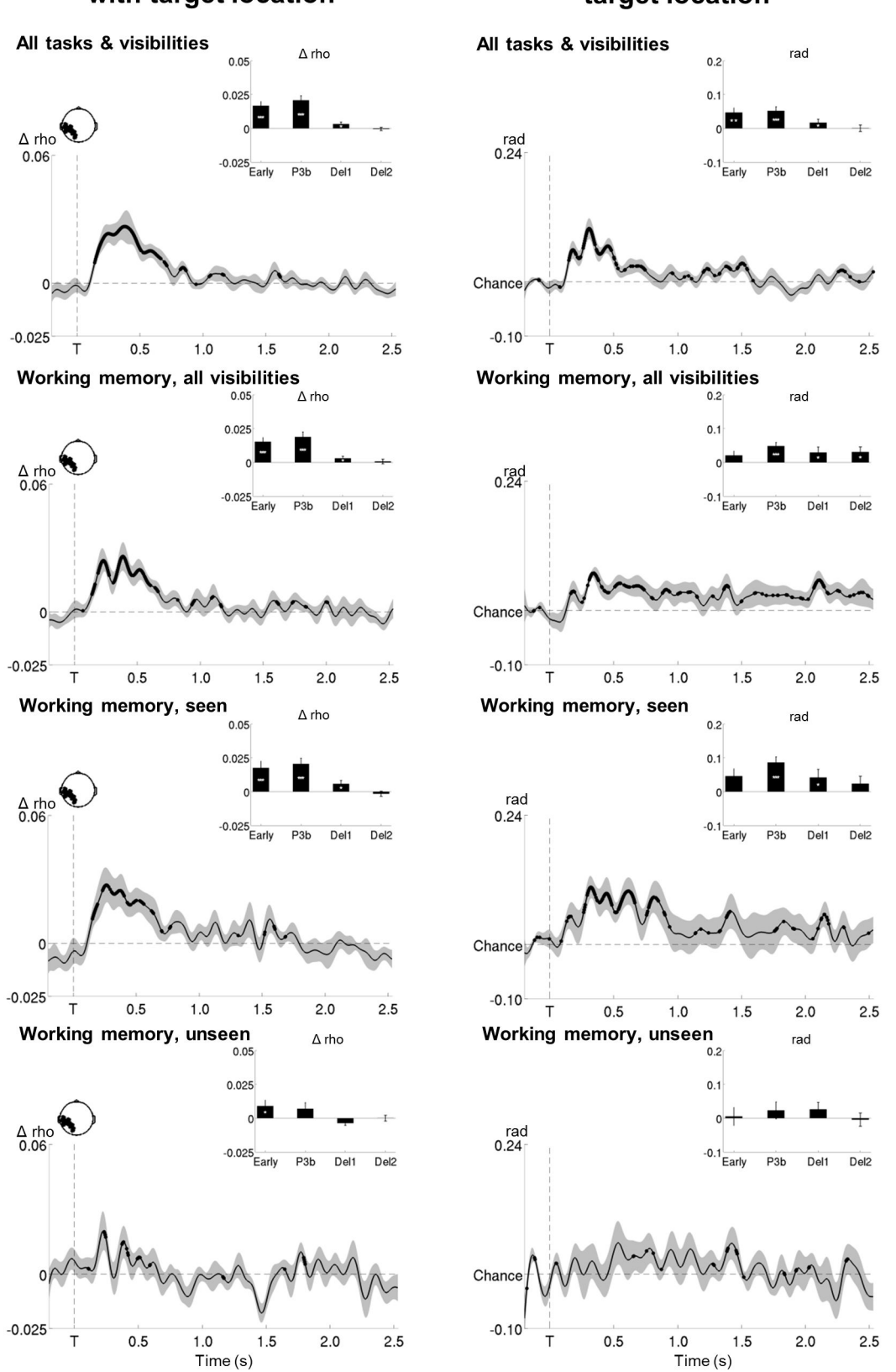

Figure 5 – Figure Supplement 3

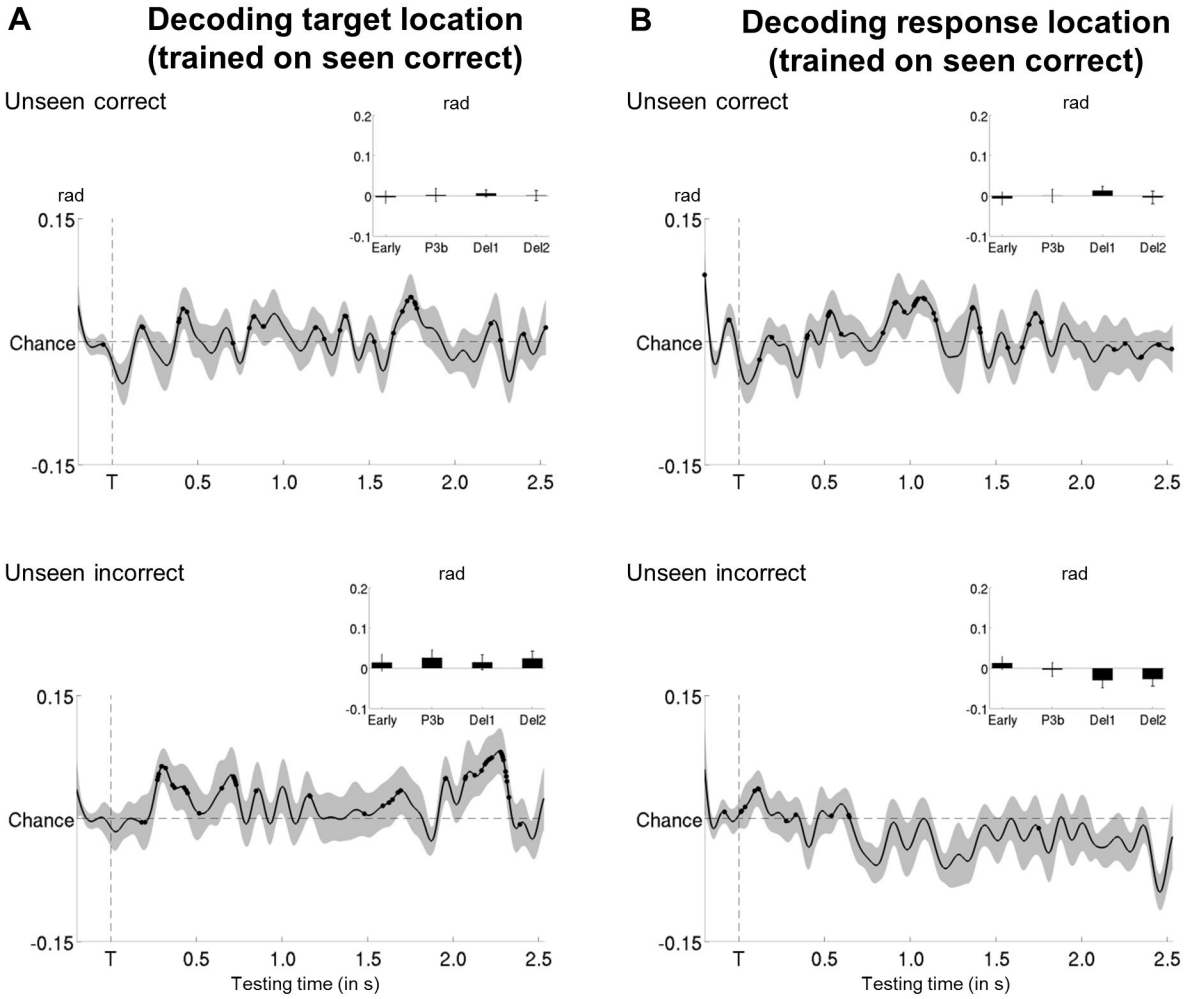

Figure 6 – Figure Supplement 1

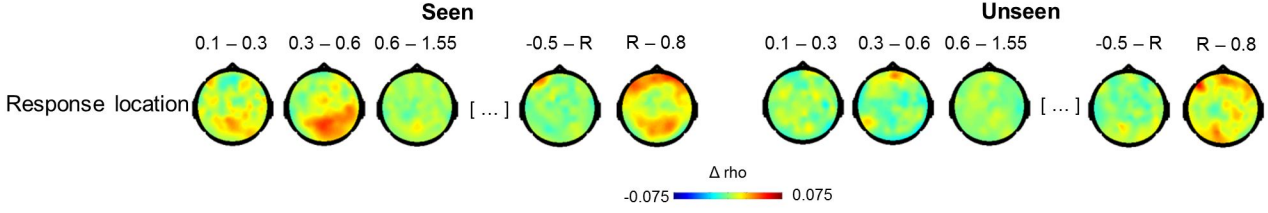

Figure 6 – Figure Supplement 2

A Circular-linear correlations with response location

B Decoding response location